Escola d'Enginyeria de Telecomunicació i Aeroespacial de Castelldefels
UNIVERSITAT POLITÈCNICA DE CATALUNYA

TREBALL FINAL DE GRAU

TFG TITLE: Fluidic Active Flow Control of Boundary Layer Separation on Supercritical Airfoil

DEGREE: Bachelor's degree in Air Navigation Engineering

AUTHOR: Jordi Jurado Chillida

DIRECTOR: Fernando Pablo Mellibovsky Elstein

DATE: July 08, 2019

Títol: Fluidic Active Flow Control of Boundary Layer Separation on Supercritical Airfoil

Autor: Jordi Jurado Chillida

Director: Fernando Pablo Mellibovsky Elstein

Data: 08 de juliol del 2019

Resum

Actualment, durant les fases crítiques de vol com serien l'aterratge, enlairament o aproximació, els avions necessiten sistemes que ajudin a millorar la sustentació.

Centrant-nos en l'ala, el perfil alar és una secció transversal d'aquesta, per tant, podem trobar diversos dissenys i configuracions amb diferents propietats segon les necessitats. Concretament, molts dels avions utilitzen perfils NACA però, des de fa uns anys, avions comercials com el A380 o B787 o militars com el C-17 utilitzen perfils alars de la categoria SC (supercrític) que milloren la eficiència global.

Particularment, aquest treball de fi de grau, es centra en l'anàlisi del flux a través de la capa límit en perfils supercrítics quan l'avió està volant a Reynolds baixos. Les simulacions s'han realitzat a diferents angles d'atac per analitzar el comportament i els límits del perfil.

Amb aquest anàlisi s'assenten les bases per tal de proposar sistemes de control actiu del flux amb la finalitat de reduir els sistemes mecànics de l'avió i conseqüentment, el pes, manteniment i problemes relacionats. Per exemple, durant un aterratge a BCN, en comptes de veure i escoltar com un sistema complex es desplega, veurem un jet que aportarà el mateix efecte.

Durant l'estudi es fan diverses simplificacions, possibles gràcies a treballar a baixos Reynolds, com el fet de treballar amb flux incompressible. També es treballarà amb un perfil aproximat al supercrític sobre el que volem extrapolar els resultats.

Sobre les simulacions, s'utilitzen programes com Gmsh, Nektar++ o Paraview per al processat per tal d'obtenir resultats numèrics.

Finalment, després d'analitzar els resultats, es definirà l'angle òptim per activar el sistema de control. En referència a aquest, s'implementarà un control actiu del flux per tal de recuperar la sustentació.

Title: Fluidic Active Flow Control of Boundary Layer Separation on Supercritical Airfoil

Author: Jordi Jurado Chillida

Director: Fernando Pablo Mellibovsky Elstein

Date: July 08, 2019

Overview

Presently, during critical phases of flight like takeoff, landing or approach, aircrafts need systems as flaps or slats that helps them to improve lift. Those, hydraulic or mechanical, are deployed during these phases in order to increase the wing surface and consequently, lift.

Focusing on the wing, an airfoil is a cross-sectional shape of it; therefore, we can find many configurations or designs with different properties. Specifically, many airplanes use NACA series but, a few years ago, commercial aircraft like Airbus A380 or Boeing 787, or military aircrafts like Boeing C-17 Globemaster are using Supercritical NASA (SC) that improve the global efficiency.

In particular, this final degree project is focused on the analysis of the flow on the boundary layer in supercritical airfoil when the airplane is flying at low Reynold numbers. This analysis has been done at different angle of attack in order to analyze the behavior and limits of this airfoil.

With this study, basis is established to design a fluidic active flow control with the purpose of reducing aircraft mechanical systems and its problems related with weight, maintenance and failures. For example, when we will be landing at BCN, instead of listen and see a complex system deploying on the wing, we will see a jet on the wing that makes the same effects.

Many simplifications have been done possible because we are working at low Reynolds. One of the most important is to work with incompressible flow. Also, an approximation of the supercritical airfoil selected to process and study the behavior is done.

About simulations, software like gmsh, Nektar++ or Paraview has been used for the processing to obtain numerical results.

Finally, after analyzing simulations results, the optimal angle to deploy the systems is defined. And for this, the fluidic active flow control is going to be implemented to recover the lift.

INDEX

LIST OF FIGURES

LIST OF TABLES

INTRODUCTION

On the first decades of aviation, the aim was to fly as faster and longer as possible designing powerful engines. After that, security and reliability were the essential objectives. From 50s, aviation opened a new research field focused on efficiency without losing security that it still remains the main objective. The aim of that was to maintain performance and decrease consumption and costs. In this line, as we will see, during 70s new flow control systems were developed. At this point, active flow control appeared. The objective is to reduce weight and mechanical systems modifying the flow on the boundary layer without deploying the conventional systems. It seems ideal but there are many problems related with security and approvals because you have to implement a new system into planes that fly safety with the conventional ones.

So, in this line, many projects have been done and some big companies are developing different active flow control methods. Before the complex programs and studies, there is a first step related to the behavior of the airfoil during the critical phases and how the active flow controls systems improve lift.

In this way, this project analyzes the behavior of a specific airfoil widely used in the newest commercial and military airplanes (supercritical airfoil) when they are flying at low Reynolds. That is in the critical phases of flight: takeoff, landing or approach. Working at low Reynolds we can use numerical solutions because we avoid the turbulence scenario that appears at higher values. At this low number we are able to solve exactly the flow and the results are good enough even if the field used is not really similar to the usual aerodynamics.

As a reference planes that have this kind of airfoil (Supercritical NASA), as it was mentioned, there are commercial like Airbus A380 or Boeing 787, or military like Boeing C-17 Globemaster.

In particular, the main aim is to analyze the boundary layer detachment at different angle of attack and propose a flow control system on the optimal angle. Other objectives to accomplish before achieving the main, are working with software that allow to mesh airfoils, simulate flows and render them. Also, have a good knowledge about active flow control systems.

Once the objectives are defined, the project is divided in 4 main chapters. The first one is the theoretical background where the general flow conditions and simplifications are explained. This is the part related to the simplification from NASA airfoil to a NACA 4-digit in order to simplify the computational code. Because with it, we can use numerical expressions. After that, concepts like boundary layer detachment and vortex shedding are explained. Finally, an important concept is defined, the hysteresis, that shortly it is a phenomenon where there is coexistence of different solutions at same angle.

The next chapter consist in explaining the simulation process. This contains all related with the software used and its particularities. In particular, the ones used has been “gmsh” for mesh developing, “Nektar++” for simulations processing, “octave” for graph designing and “paraview” for visualization.

The third chapter is focused on the simulations result and the analysis of them. In this, aerodynamical forces has been analyzed on the first section. Then, these results give us an important conclusion, the hysteresis on this airfoil at a certain angle of attack. Consequently, this is studied and most of the project is changed to analyze the phenomenon. The last section analyses the boundary layer and vortex shedding taking into account that we have found hysteresis.

The fourth chapter is related to the active flow control. Once we know that a flow control is needed, it is time to propose it and view the results of the airfoil with these modifications. In this way, an active flow control with a synthetic jet is proposed after an explanation about this topic. And finally, are mentioned the difficulties related to the jet implementation on a cambered airfoil and why it has not been possible to simulate it.

Finally, the main acronyms and definitions used are:

- AoA: Angle of Attack
- AFC: Active Flow Control
- Cl: Lift coefficient
- Cd: Drag coefficient
- Re: Reynolds number
- SC Airfoil: Supercritial Airfoil

CHAPTER 1. THEORETICAL BACKGROUND AND SIMPLIFICATIONS

1.1. Flow conditions

1.1.1. Reynolds Number

One of the basics hypotheses is to determine an acceptable Reynolds number. In this case, low Reynolds number are applicable because is intended to simulate the behavior of the airfoil when slats or flaps are needed to increase lift. This happens in critical phases of flight as takeoff, approach or landing.

This case intends to study different angles of attack (from 3 to 12 degrees) for a common Reynolds number. The computation is going to be done for a speed of 160 knots. This is the standard final approach speed for narrow or wide-body planes in Barcelona Airport as we can find in Appendix IV of AIP Barcelona Airport [5]. Also, as we are in approach phase, ISA conditions are taken. Remembering, those are: temperature of +15ºC, 101.325 Pa of pressure and 1,225 Kg/m^3 for air density.

- V (velocity) = 160 kts ≈ 82 m/s ≈ 300 km/h
- C (chord) = 1 m
- v (kinematic viscosity) = 1.48 * 10^{-5} m^2/s

$$Re = \frac{V \cdot c}{\nu} = 554.000 \quad \textbf{(1.1)}$$

The calculated Reynolds number is around Re=5.5*10^5. For this case, we want a low enough Reynolds to be in the laminar region on the boundary layer once the transition passed. So, the Reynolds to be used will be Re=5.500.

The range of AoA angles is because in Barcelona Airport AIP, the descend angle is 3º. But as it is known, the AoA is different than the descend angle as it can be seen shortly in the figure 1.1. extracted from the web “studentpilotnews.com”.

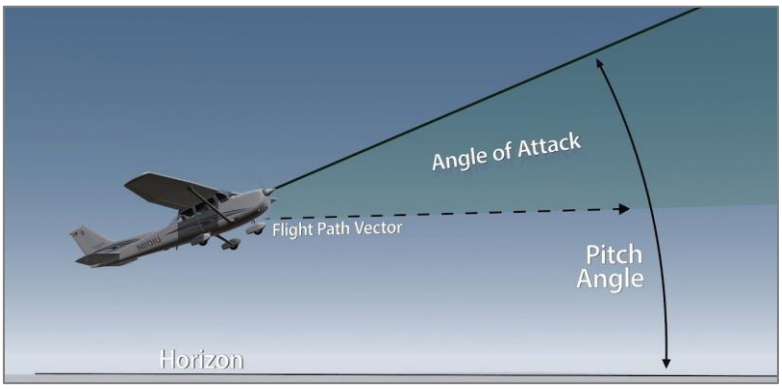

Figure 1.1: Difference between flight path and AoA

1.1.2. Navier-Stokes equations

As a low Reynolds is considered, also is feasible to consider incompressible flow (velocity gradient it's equal to zero). And as it will be seen, the simulation will take order when the transition regime is passed and we can consider stationary flow distribution. With these approximation, Navier-Stoke equations can be considered for the simulation in a 2D scenario. See the equations below:

$$\frac{\partial V}{\partial t} + V \cdot \nabla V = -\nabla p + \nu \nabla^2 V \quad \textbf{(1.2)}$$

$$\nabla \cdot V = 0 \quad \textbf{(1.3)}$$

Where *V* is the velocity, *v* the kinematic viscosity and *p* the specific pressure.

As it will be seen, the resolution for this equation and the others, in order to obtain numerical results, it will be done with Nektar++ that take into account all variables.

1.2. Airfoil Simplification

This project is focused on supercritical airfoils but, due to high complex shapes, materials and programs available to perform simulations, a NACA 4-digits approximation has to be done.

1.2.1. Supercritical Airfoil: NASA SC20412

Supercritical Airfoil concept was developed during 1960s and the first test flight was in the early 1970s on a F-8 Crusader.

After this short introduction, the main differences of Supercritical Wings (SCW) with conventional airfoils are: flatter on the top, rounded on the bottom and the upper trailing edge is marked with a downward curve in order to restore lift lost by the upper surface. This shape allows to delay the onset of the shock wave reducing aerodynamic drag associated with boundary layer separation. Therefore, the aircraft is capable to reach higher velocities, increase efficiency and reduce fuel consumption.

Nowadays, SCW are used in most of large aircrafts. In commercial aviation like A380, B787 or B777, and military aviation like C-17 or A400M.

In this this project, NASA SC20412 used in C-17 Globemaster III has been selected due to numerous studies has been done along this aircraft.

1.2.2. NACA 4-digits approximation: NACA 2412

As can be seen below, the complexity in terms of shape and its implementation in a meshing program (in this case, gmsh) of a supercritical airfoil force us to use a 4-digit NACA simplification.

To achieve a good level of similarity, NACA 2412 is going to be used. To choose this airfoil, firstly the digit meaning was analyzed:

NACA MPXX → NACA2412

- M = Maximum camber divided by 100 = 0.02c
- P = Maximum camber position divided by 10 = 0.4c
- XX = Thickness divided by 100 = 0.12

The most important digits to have a good approximation are the first two because these give us the curvature of the airfoil. One of the development principles for supercritical airfoil.

Once the shape is similar, it is time to compare the lift and drag coefficients and its behavior at same conditions. This is shown below with both airfoil profiles, first with a shape comparison (figures 1.2 and 1.3), and second with graph coefficients (figure 1.4). All this graphs and images has been generated with *"Airfoil tools"*[11], a web application with a wide airfoil database and the possibility to generate and compare your own airfoils.

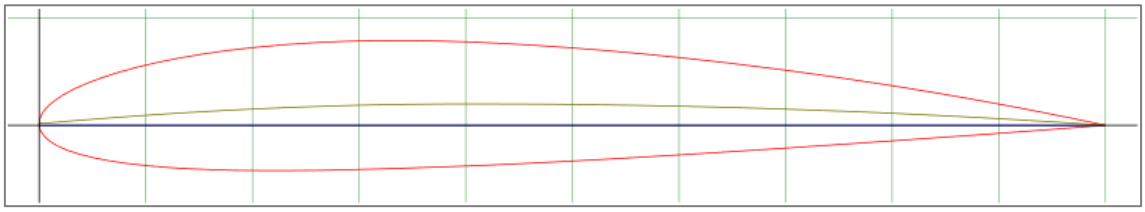

Figure 1.2: NASA SC20412

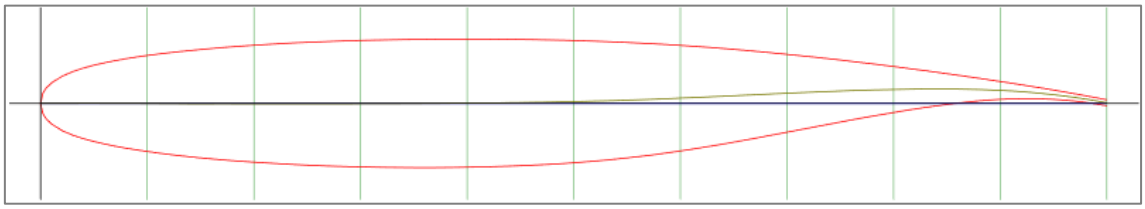

Figure 1.3: NACA 2412

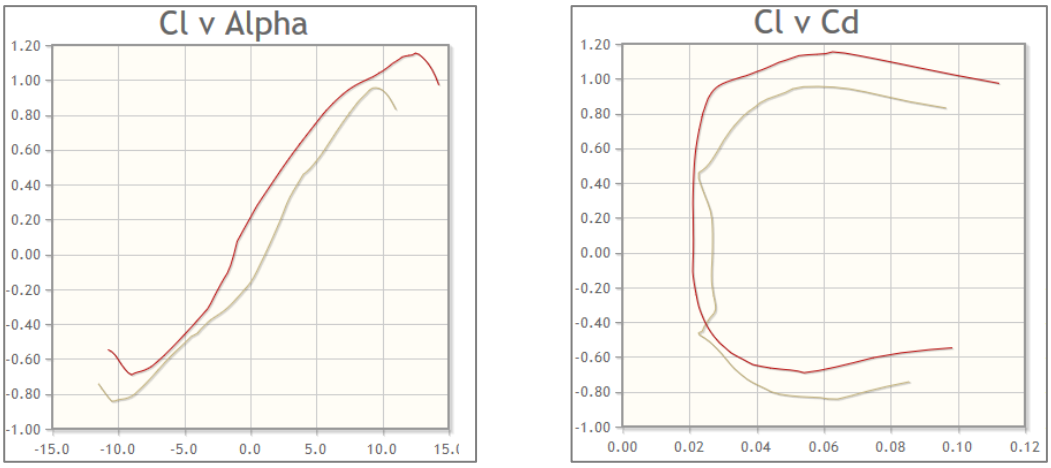

Figure 1.4: Cl and Cd vs Alpha. (Red: NACA2412, light Brown NASA SC20412)

For finishing this chapter, it can be established that supercritical airfoil NASA SC20412 can be simplified with a NACA2412. The shape is quite similar and the most important, lift and drag coefficients are reaching values accepted to start a flow simulation along the airfoil.

After this conclusion, the equations that we will use to plot and compute a NACA 4-Digit can be presented:

$$\begin{cases} y_c = \frac{m}{p^2}\left(2p\left(\frac{x}{c}\right) - \left(\frac{x}{c}\right)^2\right), & if\ 0 \le x \le pc \quad \textbf{(1.4)} \\ y_c = \frac{m}{(1-p)^2}\left((1-2p) + 2p\left(\frac{x}{c}\right) - \left(\frac{x}{c}\right)^2\right), & if\ pc \le x \le c \quad \textbf{(1.5)} \end{cases}$$

where:

- *m* is the maximum camber (100 m is the first of the four digits),
- *p* is the location of maximum camber (10 p is the second digit in the NACA xxxx description).

1.3. Boundary layer detachment and Vortex Shedding

Other phenomena to be studied in order to propose an active flow control (AFC) is the detachment of the boundary layer and vortex shedding.

As a first concept, the boundary layer is the region near to airfoil where, due to forces like viscosity, a velocity field is generated. Zero at walls, until a value far enough in order to don't perceive the effects.

After that, the concept of boundary layer separation or detachment, occurs when the portion of the boundary layer closest to the wall or leading-edge reverses in flow direction. The separation point is defined as the point between the forward and backward flow, where the shear stress is zero. See an example in figure 1.5.

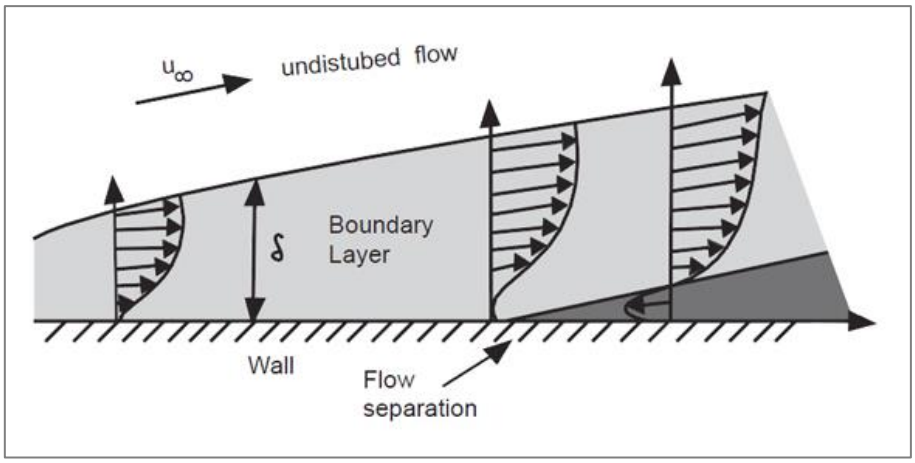

Figure 1.5: Boundary layer along an airfoil

From left to right, the first velocity field belong to the instant where all flow is passing uniformly through the airfoil. But, if we focus on the other fields, we arrive at the searched concept, the boundary layer separation.

This phenomenon occurs when, while the angle of attack is progressively increased, the flow is not capable to be on attached on the wall of the airfoil. An adverse pressure gradient is generated and the velocity is moved in opposite direction, causing separation on the boundary layer and a velocity field similar to the last figure.

The boundary layer detachment and the apparition of the adverse velocity field cause a flow recirculation that generate a swinging wake as it can be seen in the figure 1.6 [10]. Vorticity is extended along the wake airfoil. It is called shedding vortex and an instability area is generated from the boundary layer detachment.

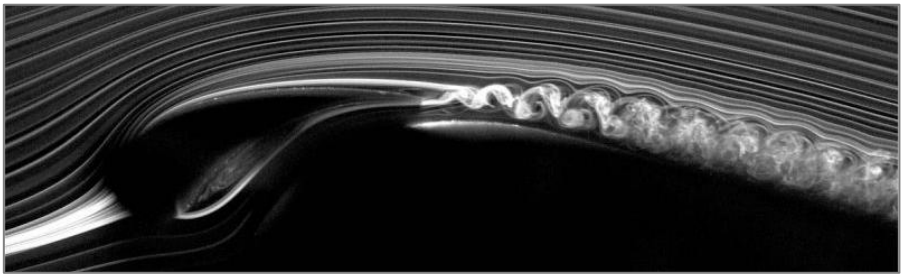

Figure 1.6: Vortex Shedding

Those phenomena can cause stall situation on the airfoil and vibrations along the structure that can affect the efficiency. For this reason, these points are studied in detail and reattachment of boundary layer systems are designed.

1.4. Hysteresis

We can define this phenomenon called hysteresis as the region where, depending the initial conditions, we can find coexistence of solutions for the same angle, or for a short range of angles. In these cases, to confirm this hypothesis, is proceeded with some simulations around the suspected angle.

As we will see in chapter 3, hysteresis can be observed when decreasing the angle of attack of a wing after stall. The angle of attack at which the flow on top of the wing reattaches is generally lower than the angle of attack at which the flow separates during the increase of the angle of attack.

From the thesis “Hysterical behaviour of a NACA 0012 airfoil at ultralow Reynolds upon variation of the angle of attack”, we can see the figure 1.7 that explains hysteresis ant its double node and unstable region.

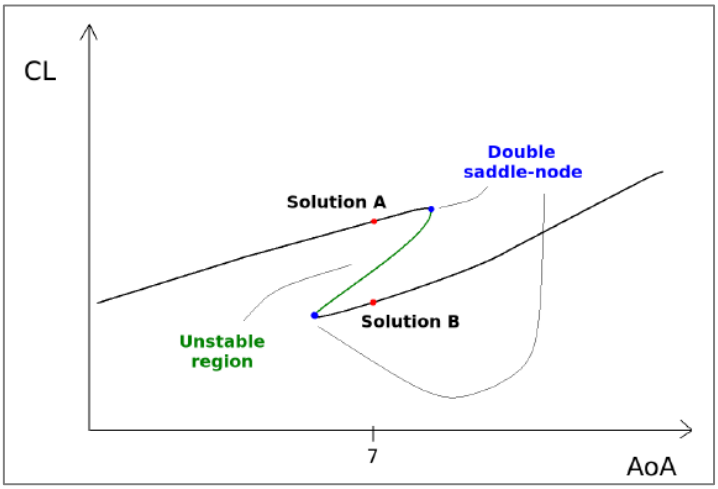

Figure 1.7: Hysteresis definition

Once the hysteresis is defined, to demonstrate its existence, as we will do, some simulations around the suspected angle will be done. These has to be starting from converged solutions and for the same angle or range of angles.

CHAPTER 2. SIMULATION PROCESSING

2.1. Pre-processing: Mesh generation

To solve Navier-Stokes equations is necessary to have available some numeric methods that allows us calculate an exact solution. Hence, the first thing we have done is generate an airfoil and a region that allow us to reach and calculate each point from its position (X and Y) during an established time or steps of time. After that, velocity and pressure fields and its behavior can be solved with the desired flow conditions. Summarizing, the area along the airfoil has to be discretized.

This process is done with software *Gmesh*. It allows to define the airfoil and design a mesh divided in different control surfaces as it can be seen in figure 2.1. To develop the mesh for our profile (NACA2412) a base "x".geo file (gmsh extension) for a NACA0012 is used. It has been extracted from the thesis *"Hysteretical behaviour of a NACA 0012 airfoil at ultralow Reynolds upon variation of the angle of attack"*. Many modifications are done because we are working with a cambered profile besides another flow, angle and airfoil conditions.

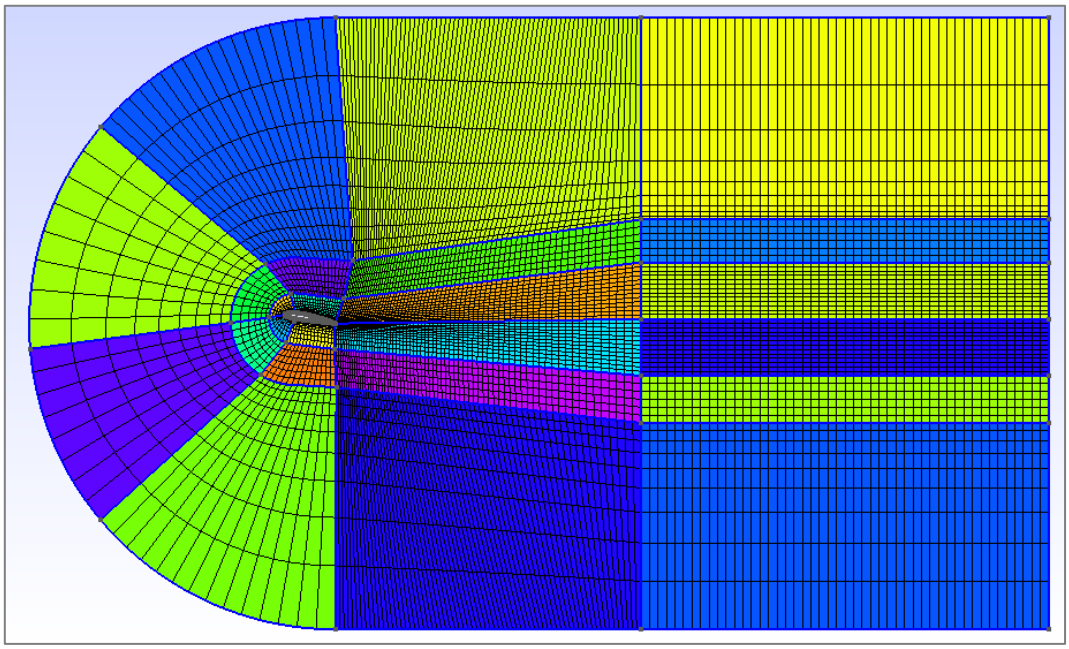

Figure 2.1: NACA2412 mesh

In order to have the maximum precision on the simulation results, the mentioned control surfaces have been divided in the next regions:

- Nearfield: This is the nearest to the airfoil where the maximum precision is desired so the density for the mesh is higher.

- Midfield: It is an area with a similar dimension in order to maintain the progression of the nearfield area without losing precision.

- Farfield: It is the widest and far away from the airfoil and is used to extend the flow condition to an area with points not affected by the airfoil shape.

- Wake region: It is the region that takes into consideration the inclination related to the AoA and the wake generated by airfoil.

- Fringe region: It is similar to the farfield region, as it is mentioned, is to have a wide region around the airfoil to don't have distortion on the walls.

From this step, the first is to adapt the code to our NACA2412 requirements. Then, make necessary changes to stand the cambered shape at different angles because some option like mesh density or progression for transfinite lines are not supported by high angles of attack. First changes are related with airfoil typology and, because the objective is to simulate different angles at a same Reynolds number, modifications on this are done (figure 2.2). Basically, we are defining the angle in radians, the coefficients of the NACA 4-digits and the number of points that will be generated to define the airfoil.

```
//****************************************
// GEOMETRY PARAMETERS
//****************************************

// CASE
aoa=10.*Pi/180; // working AoA (guides wake

// AIRFOIL
c=1; // chord
t=0.12; // max thickness (in % of chord)
m=0.02; // max camber (in % of chord)
p=0.40; // max camber position (in % of chor
tetype=0; // trailing edge type: 0: sharp; 1
N=100; // number of points defining airfoil
```

Figure 2.2: Airfoil definition code

Due to airfoil curvature, parameters associated with equidistance have to be changed. The density of the mesh is defined, higher values on the number of points along a surface defines more density and more accuracy. Different values on the upper and lower surface are proposed in order to obtain more accurate results on the upper surface and be able to detect the detachment point on the boundary layer. Those can be shortly seen on figure 2.3.

```
// AIRFOIL
Nua=21; // number of points along airfoil upper surface
ibuas=1;//2; // 0: equispaced; 1: Progression; 2: Bump
kbuas=1.01; // Progression/Bump parameter
Nuf=9; // number of points along airfoil upper surface
ibufs=1;//1; // 0: equispaced; 1: Progression; 2: Bump
kbufs=1.5; // Progression/Bump parameter
Nla=15; // number of points along airfoil lower surface
iblas=2;//2; // 0: equispaced; 1: Progression; 2: Bump
kblas=0.4; // Progression/Bump parameter
Nlf=9; // number of points along airfoil lower surface
iblfs=1;//1; // 0: equispaced; 1: Progression; 2: Bump
kblfs=1.5; // Progression/Bump parameter
```

Figure 2.3: Mesh density code

Once those changes are done, the mesh automatically adapt the point to the different angles. As it is said, the considered angles are 3, 7, 9, 10, 11 and 12. As we will see, more meshes have been generated around the angle of 10º due to unusual behavior around this angle of attack.

2.2. Processing and Post-processing

When the mesh is generated into a *.msh* file (an option in gmsh to convert the .geo file), the next software to use is *Nektar++* where the post-processing is done. Here, flow conditions are established and the mesh file has to be converted to another extension acceptable by this software (.xml). After that, data will be processed and results simulated on time. As a comment, the option to use *OpenFoam* for post-processing was considered and tried but the conversion from *Gmsh* had many problems to prepare it for many angles.

Then, for processing simulations, the solver “incompressible Navier Stokes” was used. It has mesh and flow conditions inputs processed for a specified time step. Therefore, the first step once we have the mesh file is to convert it to an acceptable format, in this case, “.xml”. This process is done with an “Utility” from Nektar++ called NekMesh. It is important to focus on the remarked parameters on figure 2.4. Considering that those are the related to the geometry and will be used in the “conditions” file for defining the control surfaces parameters. The “<composite>” is defining the specific surfaces. The important thing is that we have to be defined the same Q type definitions here and in the “<expansions>” on the conditions file.

```
        <COMPOSITE>
            <C ID="1">
E[1837,1840,1842,1844,1846,1848,1850-1851,3566,3568,3570,3572,3574,3576,357
</C>
            <C ID="2">
E[12305,12401,12497,12593,12689,12785,12881,12977,13073,13169,13265,13361,1
</C>
            <C ID="3">
E[7708,7705,7702,7699,7696,7693,7690,7687,7684,7681,7678,7675,7672,7669,766
</C>
            <C ID="4">
E[10157,10155,10152,10149,10146,10143,10140,10137,10134,10131,10128,10125,1
            <C ID="5">
E[1182,1185,1187,1189,1191,1193,1195,1197,1199,1201,1203,1205,1207,1209,121
</C>
            <C ID="6">
E[3034,3036,3038,3040,3042,3044,3046,3048,3050,3052,3054,3056,3058,3060,306
</C>
            <C ID="7"> Q[0-1691,5264-5695,6608-7039] </C>
            <C ID="8"> Q[1692-2105] </C>
            <C ID="9"> Q[2106-2819,5696-5983,7040-7327] </C>
            <C ID="10"> Q[3717-4080] </C>
            <C ID="11"> Q[4978-5263] </C>
            <C ID="12"> Q[2820-3716,4081-4977,5984-6607,7328-7951] </C>
        </COMPOSITE>
```

Figure 2.4: Airfoil definition code

As mentioned, the second file needed to run the simulation is the “conditions”. This kind of files, in accordance with *Nektar*++ manuals and tutorials [8] for incompressible flow and particularizing on this case, is generated on a tree composition, containing the next sections and variables:

- Expansions: Defines each domain for control surfaces as we can see in the figure 2.5. Also, number of nodes are defined, in this case, lower to be possible to run all simulations for the cambered airfoil. As we told, the definitions are the same that in the figure 2.4.

```
<EXPANSIONS>
  <E COMPOSITE="C[7]" NUMMODES="4" TYPE="MODIFIED" FIELDS="u,v,p" /> <!-- FarField -->
  <E COMPOSITE="C[8]" NUMMODES="4" TYPE="MODIFIED" FIELDS="u,v,p" /> <!-- UpperMidFieldWake -->
  <E COMPOSITE="C[9]" NUMMODES="4" TYPE="MODIFIED" FIELDS="u,v,p" /> <!-- MidFieldExceptUpperWake -->
  <E COMPOSITE="C[10]" NUMMODES="4" TYPE="MODIFIED" FIELDS="u,v,p" />  <!-- UpperNearField -->
  <E COMPOSITE="C[11]" NUMMODES="4" TYPE="MODIFIED" FIELDS="u,v,p" />  <!-- LowerNearField -->
  <E COMPOSITE="C[12]" NUMMODES="4" TYPE="MODIFIED" FIELDS="u,v,p" />  <!-- WakeRegion-->
</EXPANSIONS>
```

Figure 2.5: Expansions definition

- Conditions: Simulation typology and other specific parameters are controlled with the next subsections:

  - Solver Info: Indicates what solvers will be used to generate the simulations. In particular, we can find the solver “Unesteady Navier Stokes” that contains the main equation to solve the Navier-Stokes solutions. Also, the *solver type*: “Velocity Correction Scheme” that contains the process to solve them. All solvers used are shown in the figure 2.6.

```
<SOLVERINFO>
  <I PROPERTY="SOLVERTYPE"              VALUE="VelocityCorrectionScheme"/>
  <I PROPERTY="EQTYPE"                  VALUE="UnsteadyNavierStokes"    />
  <I PROPERTY="Projection"              VALUE="Continuous"              />
  <I PROPERTY="EvolutionOperator"       VALUE="Nonlinear"               />
  <I PROPERTY="TimeIntegrationMethod"   VALUE="IMEXOrder2"              />
  <I PROPERTY="Driver"                  VALUE="Standard"                />
  <I PROPERTY="AdvectionForm"           VALUE="SkewSymmetric"           />
  <I PROPERTY="Extrapolation"           VALUE="Standard"                />
</SOLVERINFO>
```

Figure 2.6: Solvers used

  - Parameters: In this section is included data related with simulation times, steps, checks and flow velocity controlled by Reynolds number (Re = 5500).

  - Variables: Defines the control variables. In this case, horizontal (“u”) and vertical (“v”) velocity and pressure (“p”).

- Boundary Regions: They are defined in accordance with different contour regions. Basically, regions and points are defined with data extracted from the .xml file with mesh parameters. It is important to not confuse with the domain used in the “expansions” section.

- Boundary Conditions: Once the regions are defined, it is time to define the contour conditions. With 0 conditions at walls we start simulations. For next simulations, as we want to pass the transitory regime and find the stable solution, the obtained value in the firsts simulations are used in order to run faster because we start from a non-transitory solution. This is configurated in the subsection of “Initial Conditions” as is shown in the figure 2.7 where a specific file from a previous simulation is defined.

```
<FUNCTION NAME="InitialConditions">
  <F VAR="u,v,p" FILE="NACA9AoA_38.chk"/>
  <!--<E VAR="u" VALUE="0" />
  <E VAR="v" VALUE="0" />
  <E VAR="p" VALUE="0" />-->
</FUNCTION>
```

Figure 2.7: Boundary conditions definition

- Filters: This section defines control points like lift and drag coefficient at specific time (filter Aerofoces). We can differentiate them on the direction parameter where is defined the “X” and “Y” axes and obviously, “Z” is 0 in both cases. These coefficients have to be multiplied by 2 to obtain the real values due to ½ in the Lift formula. Also, parameters related with energy and points for measure the wake turbulence are proposed. See them on the figure 2.8.

```
<FILTERS>
  <FILTER TYPE="HistoryPoints">
    <PARAM NAME="OutputFile">naca2412Re5500.h25.1</PARAM>
    <PARAM NAME="OutputFrequency">5</PARAM>
    <PARAM NAME="Points">
      -1.1 0.0 0.0
      1.5131 0.02079 0.0
      2.5131 0.02079 0.0
      3.5131 0.02079 0.0
    </PARAM>
  </FILTER>
  <FILTER TYPE="AeroForces">
    <PARAM NAME="OutputFile">naca2412Re5500.h25.1</PARAM>
    <PARAM NAME="StartTime">0</PARAM>
    <PARAM NAME="OutputFrequency">5</PARAM>
    <PARAM NAME="Boundary">B[2,3]</PARAM>
    <PARAM NAME="Direction1">
      1 0 0
    </PARAM>
    <PARAM NAME="Direction2">
      0 1 0
    </PARAM>
  </FILTER>
  <FILTER TYPE="Energy">
```

Figure 2.8: Proposed filters

With all the files generated, we process the solver. The mean time for the simulation is around 8 hours, in order to have feasible results.

Afterwards, with the processed results, we will use *Paraview* software for processing the velocity and pressure fields. Also, we obtain the detachment points for purposing the optimal angle and point for the active flow control system.

Finally, in the figure 2.9 we can see a global view of the process.

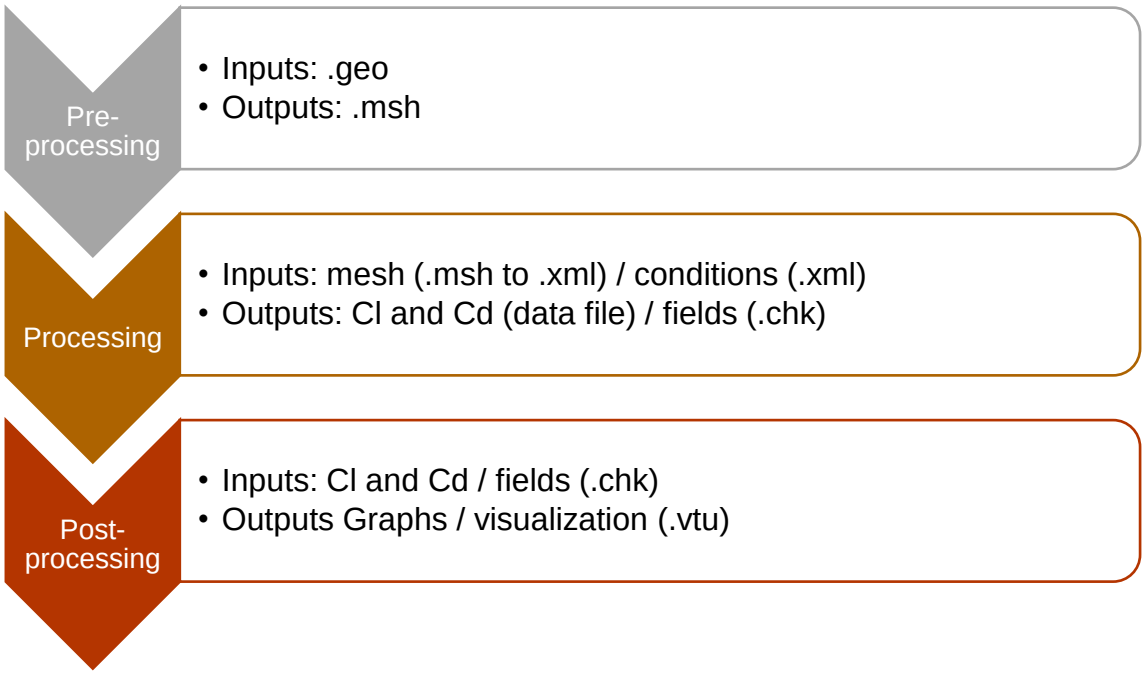

Figure 2.9: Process global view

CHAPTER 3. SIMULATION RESULTS

3.1. Lift and Drag Coefficients analysis

As the output is a data file, *Octave* software has been used to process values and develop graphs that helps us to visualize and analyze results. Once the data is processed, a graph with all angles and lift coefficient is realized. It has been done to show the behavior of airfoil in different angles and its maximum and minimum values over the mean. This range is important because, as we will see later, the solutions are defined as a periodic or quasi-periodic. This fact is really significative because the vortex shedding defined in chapter 1 becomes disturbed when the periodicity is partially broken.

The first graph to analyze is shown in the figure 3.1 and such values in table 3.1. This graph shows the behavior of lift coefficient when progressive the AoA is increased. We can see a progressive and linear increasement of the lift coefficient until 0.7 approximately that corresponds to an angle of 9 degrees. From 9 to 10 degrees the curvature is losing slope progressively.

After that point, starts an interesting region because the values lose the linearity since the angle of 10º to decrease. After decreasing for a short range of angle, lift coefficient suddenly reach values around 1.16.

Also, we can see the mean maximum and minimum values for each angle and how it range is higher than in the smooth regions. Max and min are shown because the coefficient is not a specific value, is a region where many values coexist in a short region.

Finally, from 10.5 to 12 degrees, the lift remains practically at the same values.

Due to unusual results around 10 degrees, other angles like 9.5, 9.75, 10.25 and 10.5, have been simulated and processed as we can see. This has been done in order to have accurate results in the region where unusual behavior is present.

AoA [º]	**3**	**7**	**9**	**9.5**	**9.75**
Max Cl	0.1968	0.5791	0.9067	0.9428	0.9522
Mean Cl	0.1757	0.4784	0.6743	0.6975	0.7103
Min Cl	0.1555	0.3982	0.5204	0.5359	0.5492
AoA [º]	**10**	**10.25**	**10.5**	**11**	**12**
Max Cl	0.9991	1.017	1.4899	1.4779	1.4562
Mean Cl	0.6603	0.6571	1.1680	1.1683	1.1715
Min Cl	0.3339	0.3264	0.7691	0.7783	0.7876

Table 3.1: AoA vs Cl values

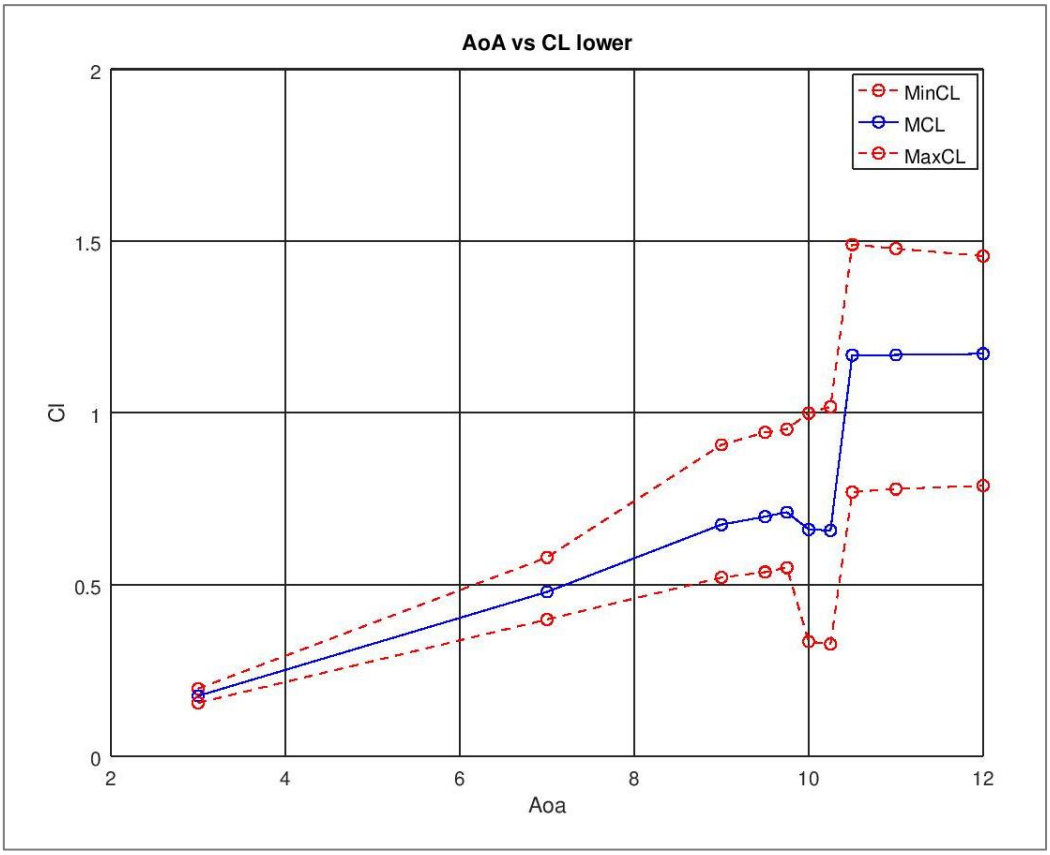

Figure 3.1: AoA vs Cl

As it is told, the graph shows more angles that we established for the airfoil study of different approach angles for same speed. This is because near the 10º angle we can see a leap on the lift coefficient, and then a recovery at higher values. Also, it is important to see how, around this region, the maximum and minimum values are dispersed in a higher range. This fact indicates us that many solutions can be reached for a same angle, and if this is true, we are on a hysteresis area.

In addition, we can see in the figure 3.2. and the table 3.2, the comparison of the lift and drag coefficients. We see how the solutions are periodic (they move in a well-defined range) and become quasiperiodic around 10 degrees. This reinforce the results obtained from the comparison AoA vs Cl where instability is detected in the near range of this angle.

AoA [º]	7	9	10	10.5	11	12
Cd	0.0970	0.1418	0.1586	0.2302	0.2405	0.26
Cl	0.4784	0.6743	0.6603	1.1680	1.1683	1.1715

Table 3.2: Mean Cd and Cl values

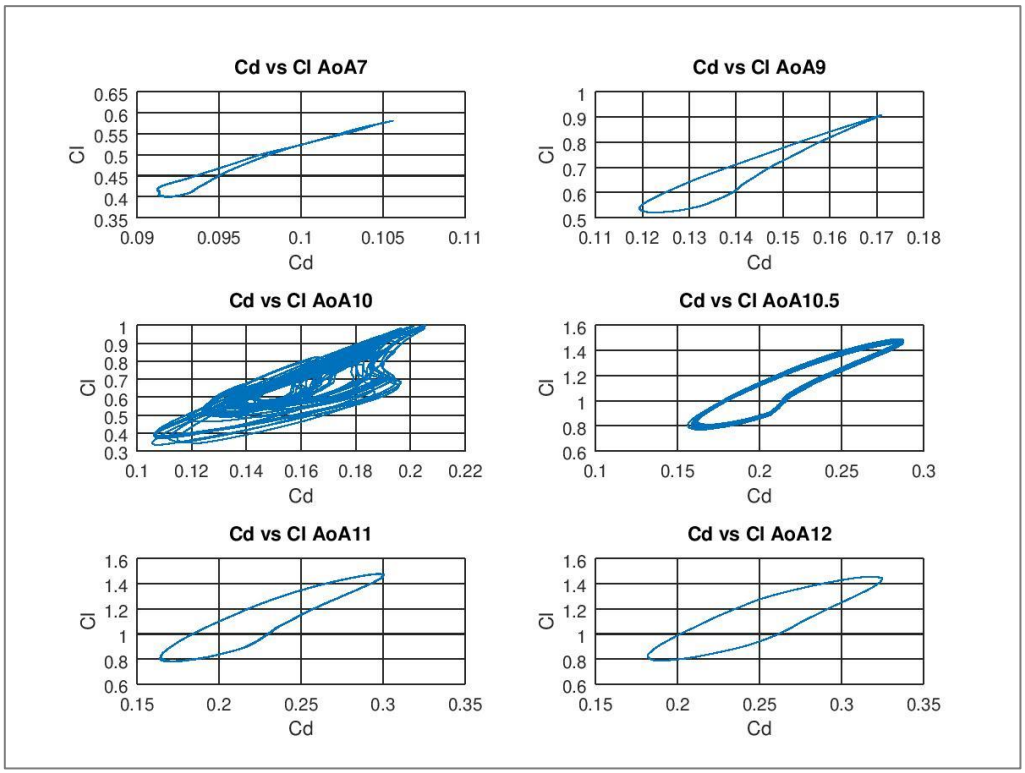

Figure 3.2: Cd vs Cl: Overall view

In the next paragraphs the variable time [s] will be introduced. This is important because the results presented comparing Cl vs AoA and Cl vs Cd are extracted removing the transitory region. This is, stable in time when no more changes or distortions are expected on the flow.

So, in order to analyze the stability and periodicity, lift coefficient vs time is plotted and extracted from the simulation results. This graph is important because we can observe how the results tend to the stability once the transitory period is passed. We have periodic results in all angles except the 10 degrees where are quasiperiodic.

As can be seen and, in accordance with the analysis done about Cl vs AoA, results are taking values into a short range. This is because coefficients are not a constant or unique value. As an exception, we find the angle near to 10º where is suspect to have hysteresis. On non-transitory time, also there is a pattern on these angles. But with unstable values, this is a quasiperiodic solution.

Firstly, on the figure 3.3 we can see an overview of representative angles. Next, on figure 3.4 and figure 3.5 are shown the 9.75º and 10.25º respectively. With these last two graphs, we can see the behavior just before and after the critical zone of 10º shown in figure 3.3. Notice how in angle variations less than 0.5 degrees we can be on periodic or quasiperiodic solutions.

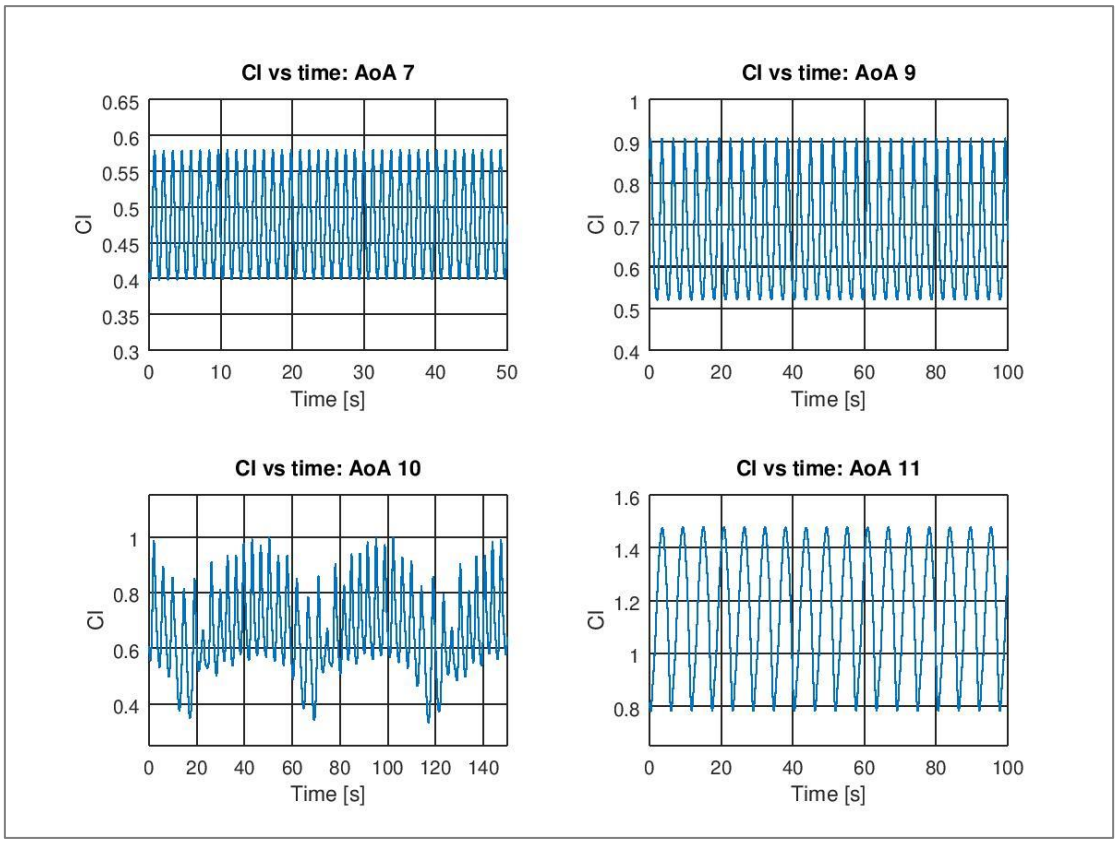

Figure 3.3: Time [s] vs Lift Coefficient: Overall view

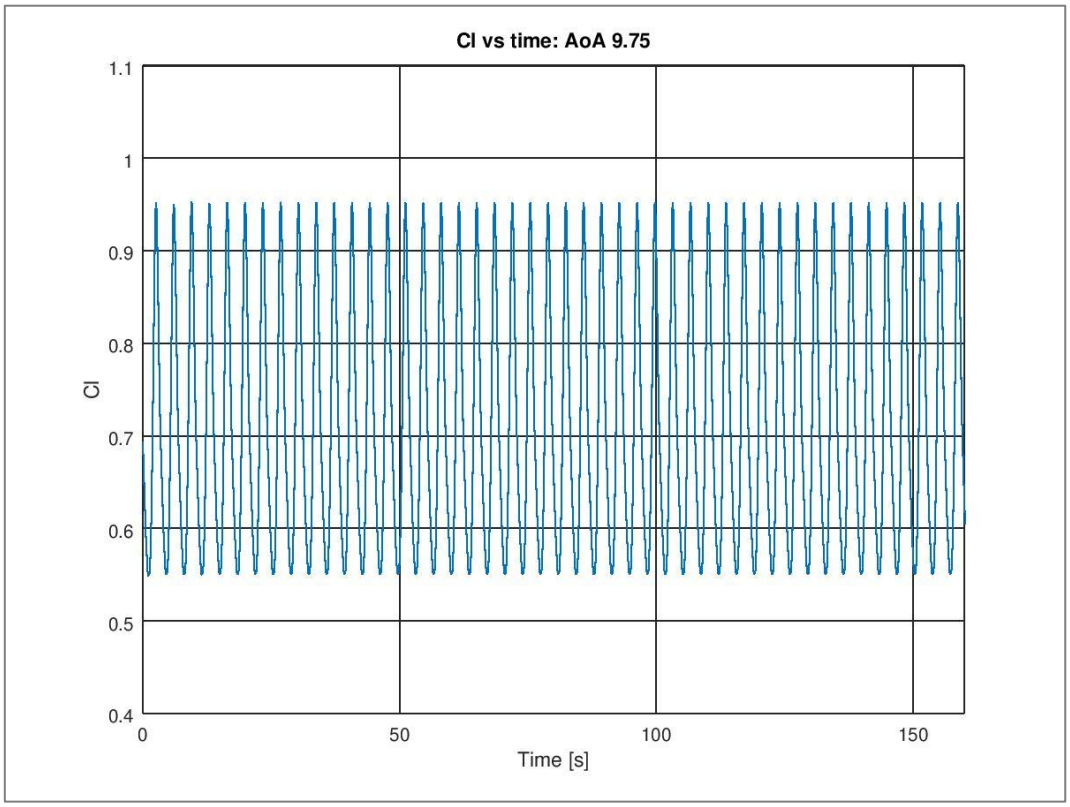

Figure 3.4: Time [s] vs Lift Coefficient: 9.75 AoA

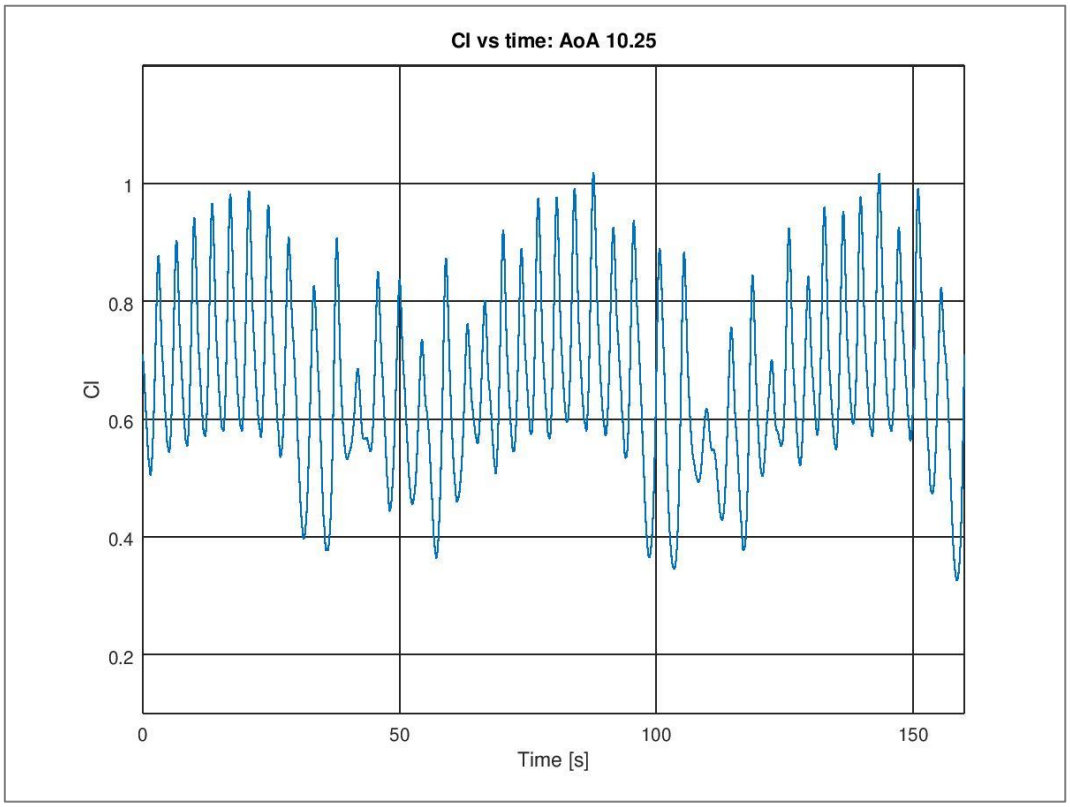

Figure 3.5: Time [s] vs Lift Coefficient: 10.25 AoA

As it has been seen in the first comparation of Cl vs Cd and supported by the analysis of Cl vs Time focused on the 10 degrees region, we come back to the comparison of lift vs drag coefficient.

We return to this graph; transitory times are removed and we focus on the area near 10 degrees. These results, on the figure 3.6, shows a short region of angles between 9.75º and 10.5º. As was told, the optimal result are graphs where values always fluctuate uniformly between a maximum and minimum. A good example can be seen for 9.75 degrees angle. Similar to previous analysis, the solutions are periodic until 10º area where a specific range of solutions cannot be delimitated and the variance of them is higher than stable angles.

It is interesting to see how the results, change suddenly from 9.75 to 10 degrees. Here, the periodicity is broken and then, returns progressively since the angle of 10.5º. So, the suspected region goes from 10 to 10.25 degrees, a really short region but can have important consequences on the airfoil stability.

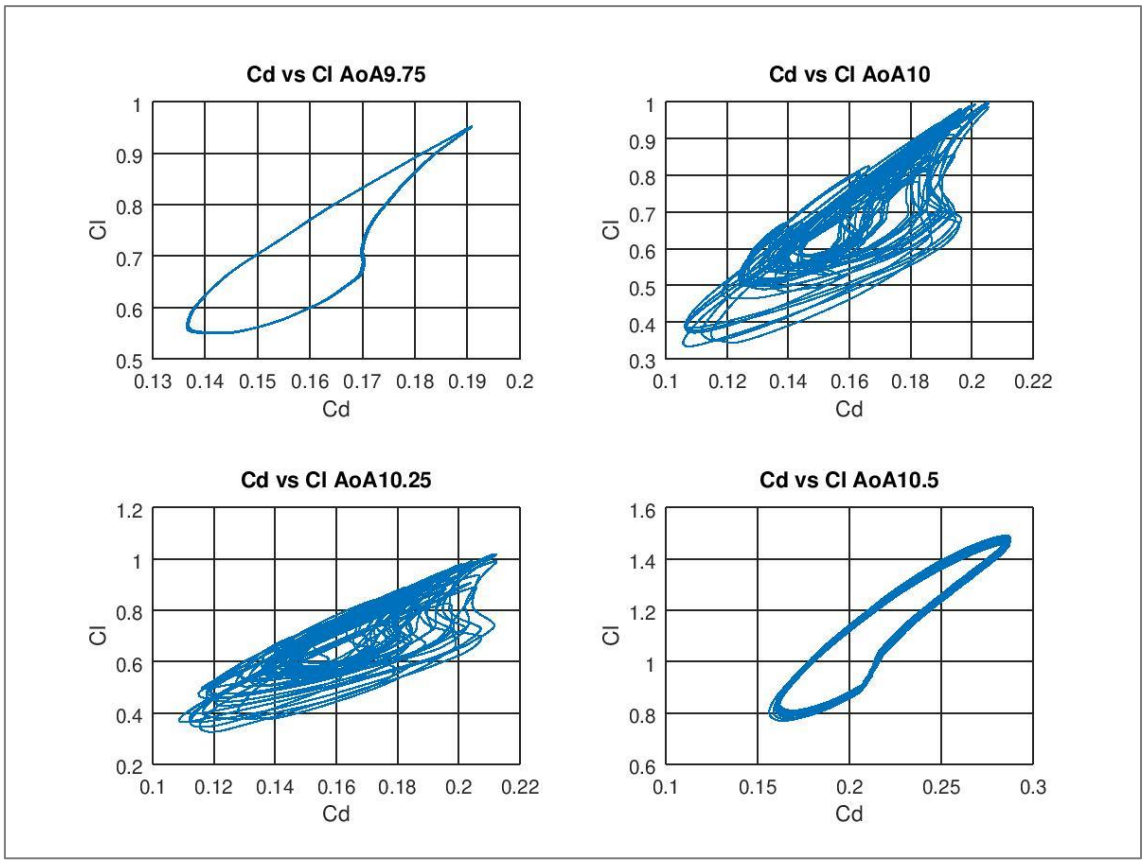

Figure 3.6: Cl vs Cd around 10 degrees region

Finally, to conclude this section, we can seriously suspect that there is hysteresis on the airfoil around 10 degrees of angle of attack. These results were not expected on the initial planning of this project. So, the next step is to run simulations near the 10º angle and not only the last done. Also, from converged solutions at higher and lower angles. Then, for summarizing, from stable solutions at lower angles for example 7, 9 or 9.5 degrees we will simulate 9.75º, 10º and 10.25º. Then, we have simulated the same another time but from higher angles like 10.5, 11 and 12 degrees in order to have enough numerical solutions to confirm the hypothesis.

3.2. Hysteresis analysis

Regarding the explanations done in the first chapter, the suspicion of hysteresis is going to be analyzed.

On the same way we have done in previous section, the first to explain is the lift coefficient vs angle of attack graph. But in this case, maximum and minimum values are removed and added a new mean Cl.

We can see in the figure 3.7 two lift coefficient lines. The green one represents the simulations around the 10 degrees starting with an initial condition of 10.5 or 11 degrees. And the blue one represents the firsts simulations seen in the chapter 3.1 did from lower angles than 10º.

This is done because, as we told, to detect hysteresis, first, we have to confirm that the airfoil NACA2412 has a different behavior in terms of lift coefficient depending the initial conditions.

Focusing the general graph in the values in the range after 9.75º and before 10.5º, we can see different values for the same angles.

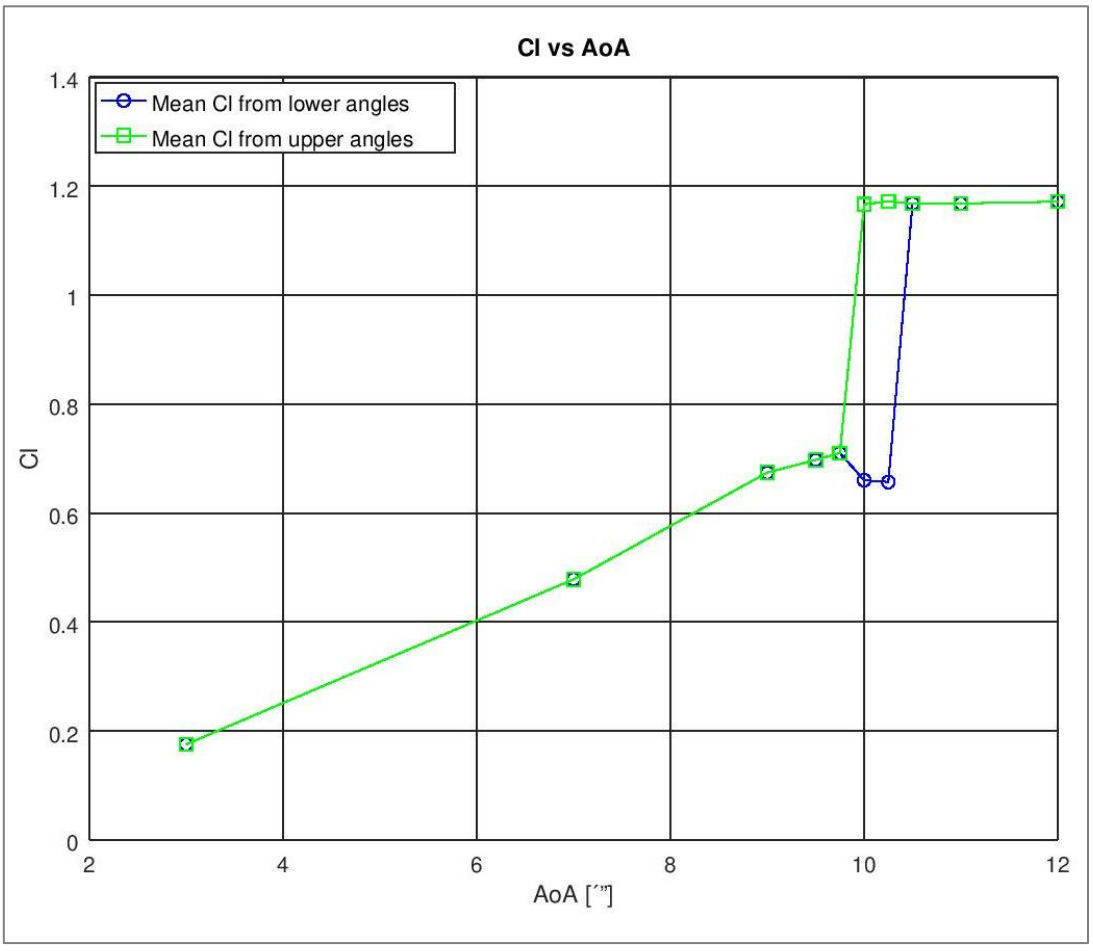

Figure 3.7: Cl vs AoA with coexistence of solutions

Hence, in this particular case of study, low Reynolds for a supercritical airfoil approximated to a cambered NACA, we have detected, as it can be seen in the figure 3.7, how coexist different solutions on the 10º area. It depends on if simulations come from initial conditions with higher or lower angles. Also is attached the table 3.3 with the numerical values of lift coefficient for each solution and angle, upper (green line) and lower (blue line) as explained.

AoA [º]	9	9.5	9.75	10	10.25	10.5	11
Cl lower	0.6743	0.6975	0.7103	0.6603	0.6571	1.1680	1.1683
Cl upper	0.6743	0.6975	0.7103	1.1666	1.1721	1.1680	1.1683

Table 3.3: Cl from lower and upper values

In the last figure, we can see how, starting from lower angles (blue solution), lift coefficient is stable until 10.25º. Where suddenly increase it value and after, the continuity is maintained. On the other hand, we started from angles like 10.5º to obtain the green solution. We can see how the Cl is decreasing progressively until the 10º where falls from around 1.16 to 0.71 values.

In addition, as it is shown in the figure 3.8 (similar to once seen in section 3.1), the solution for Cl vs Cd starting from angles lower of 10º, never converge on a stable solution. As it is done in other angles near it. Also, we can see the figure 3.9 where the solutions shown are from higher angles than 10º. It is true that have more stability, but it is not enough because the values, as it is told, fall when we arrive at certain AoA.

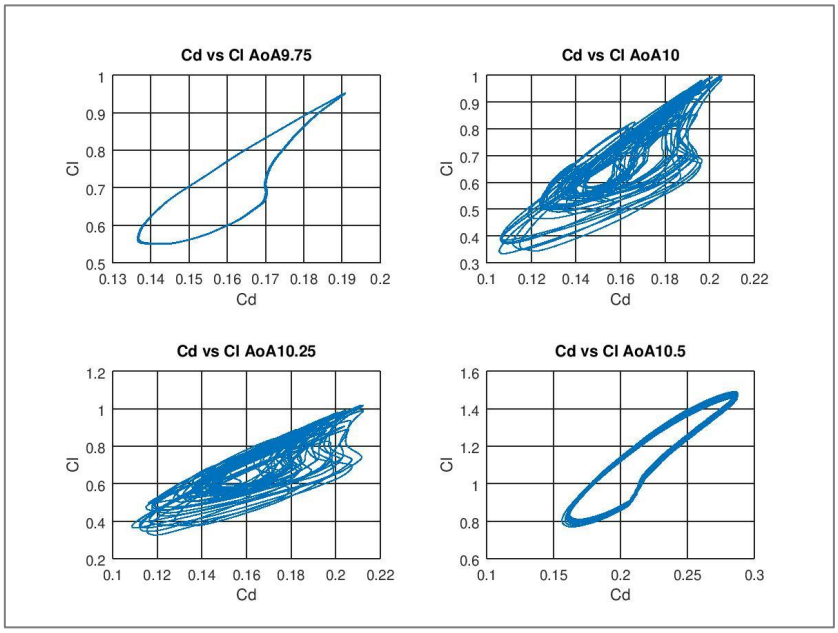

Figure 3.8: Cl vs Cd from angles lower to 10º

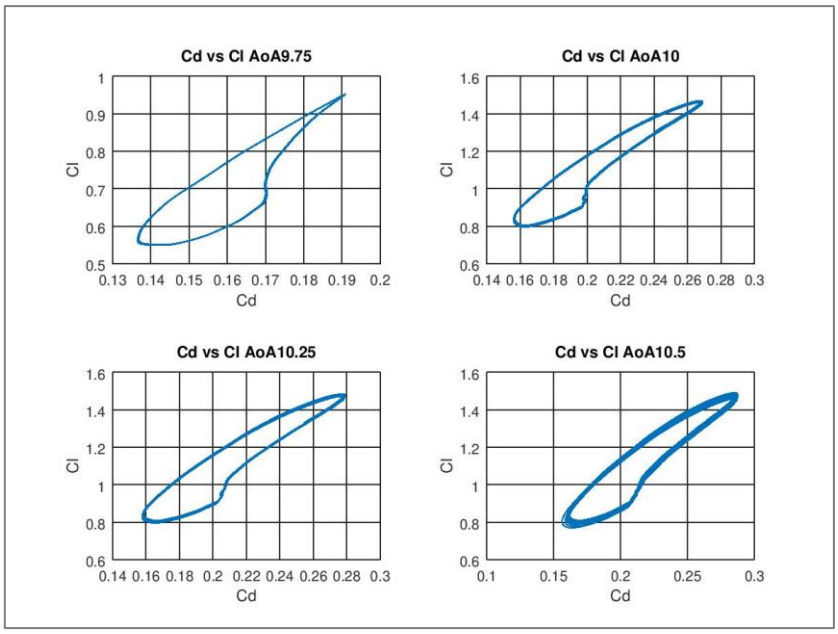

Figure 3.9: Cl vs Cd from angles higher to 10º

This last comparison is also interesting to see how the values coming from upper angles are periodic on the angles 10º and 10.25º and quasi periodic for solutions coming from lower angles.

Also, regarding another time the definition done in the first chapter. We see the double solution, the nodes in 9.75 and 10.5 degrees and the unstable region between them. So, the definition of hysteresis is accomplished.

"This quasiperiodic and solution coexistence area, allow us to conclude that in the NACA2412 airfoil, approximated from a supercritical and with approach speed (Re=5500), exist hysteresis around the 10 degrees Angle of Attack."

As we will see, the fact of finding a hysteresis area determinate us which angle we have to correct the lift. Deploying an active flow control system in order to recover the lift on the airfoil. See in the figure 3.10 the global analysis process.

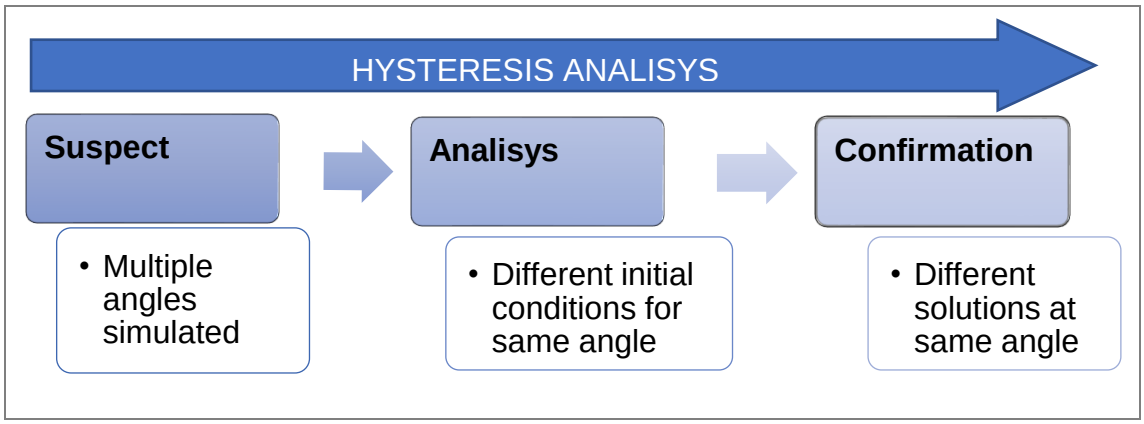

Figure 3.10: Hysteresis global analysis process

3.3. Boundary layer detachment and Vortex Shedding

Other phenomena to be studied in order to propose an active flow control (AFC) is the detachment of the boundary layer and vortex shedding. Those, combined with the detected hysteresis, determine in which angle the AFC has to be activated. Also, we can know at what point is necessary to design it to be optimal.

Related to the boundary layer and vortex shedding, we proceed to analyze the solutions obtained for the NACA2412 at different angle of attack. *Paraview* software has been used to run the file in order to create an animation based on frames. In figures 3.11 and 3.12 we can observe the velocity and pressure fields respectively for 3, 7, 9, 10, 11 and 12 AoA. Those angles are selected in order to see in detail the detachment while the AoA increases. This first simulations are done to show the wake generated, later we will specify on the point of detachment and vortex generated.

With 3º of AoA the boundary layer is attached because we can see how the velocity in the walls remains almost 0 and no inverse gradient is generated. Increasing the angle, velocity increases in the upper surface and detachments of this are generated. After 10 degrees and clearly on 12, the velocity is disturbed and the boundary layer is detached.

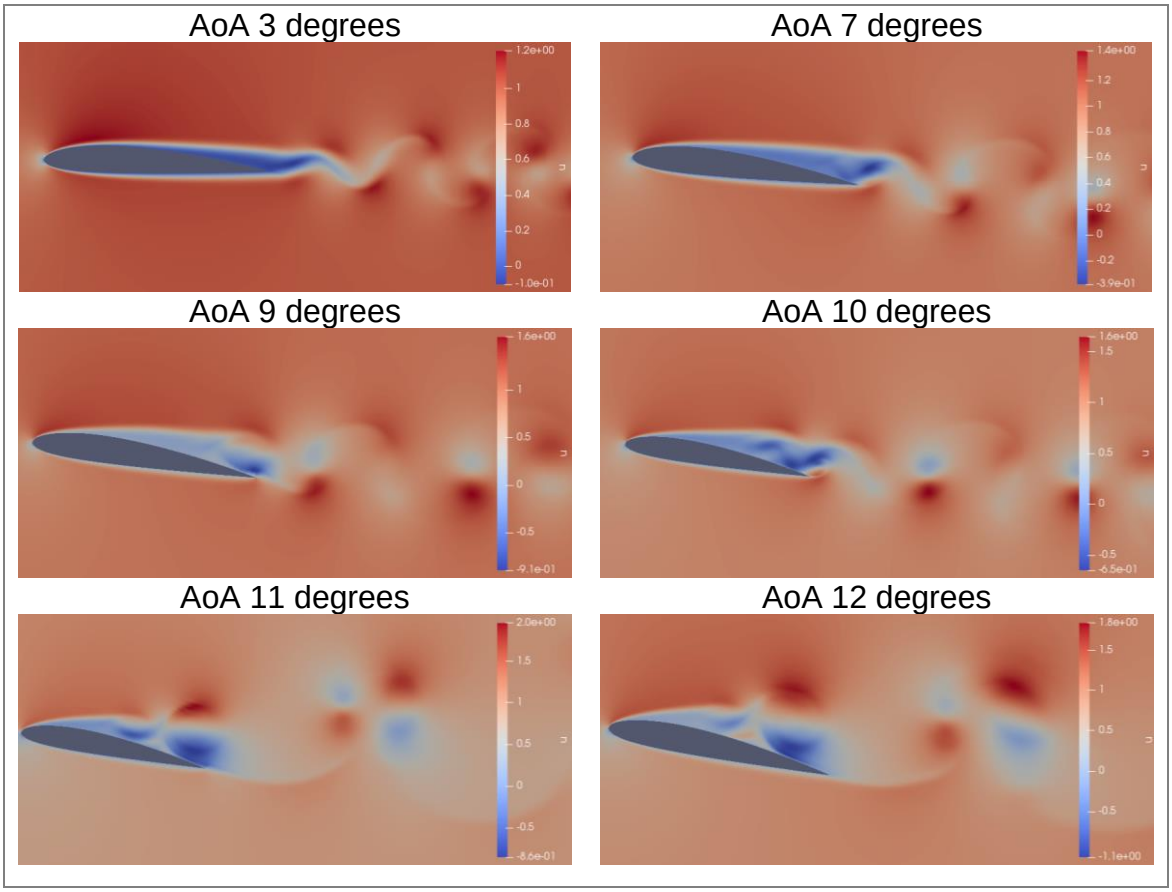

Figure 3.11: Velocity field comparation

Now, we can see the pressure field in order to talk about the pressure gradient. The one that moves the velocity in opposite direction as it has been explained in the theoretical background.

At 3 degrees the pressure is practically the same on the upper and lower surface. After that, while increases the angle, pressure is higher in the lower surface and lower in the upper. These results are in accordance with the flight theories and lift generation due to velocity around the wing.

Coming back to the results, same with velocity field, low pressure fields are generated in the upper surface breaking the constant pressure necessary to avoid the detachment of the boundary layer.

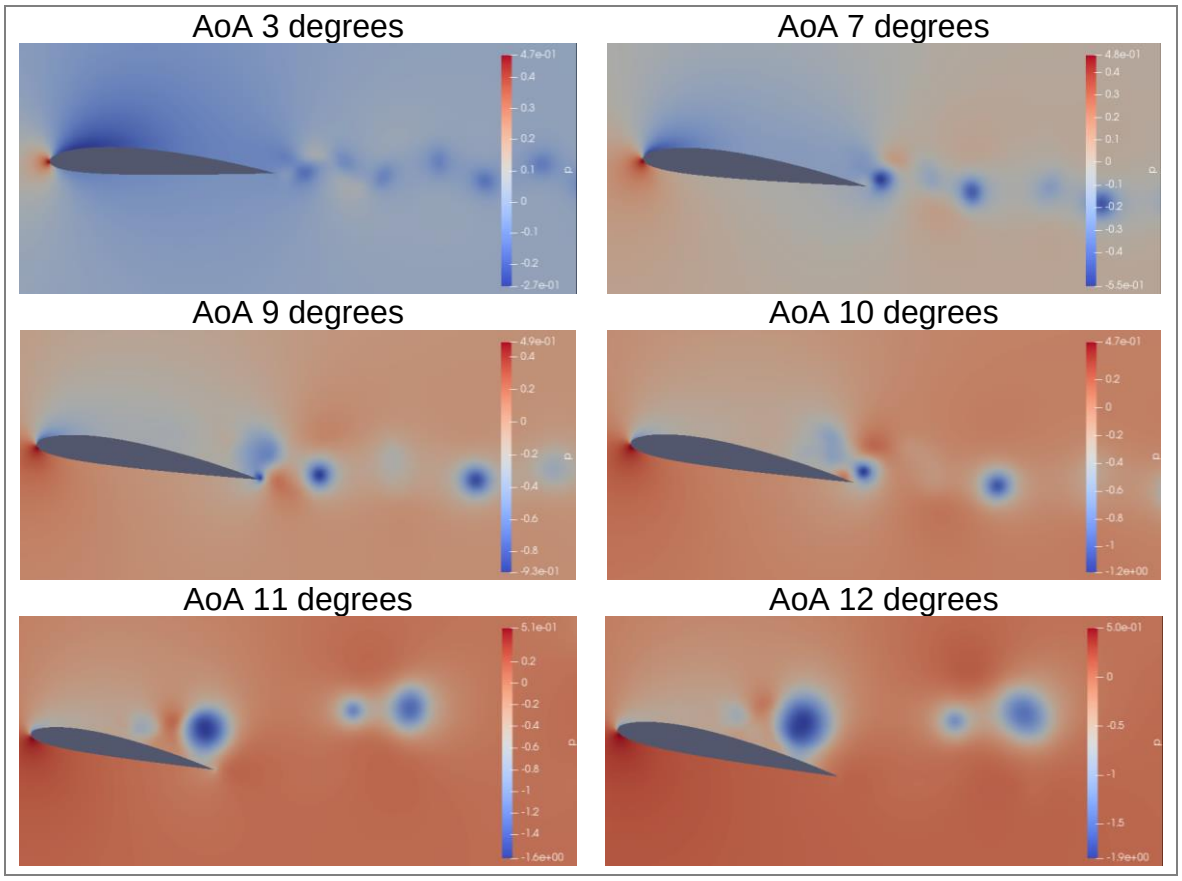

Figure 3.12: Pressure field comparation

On the other hand, we should focus on the vortex shedding and see that while the angle is increasing it becomes unstable. Specially on the angles near to 10 degrees as we can see in figure 3.13. In these images are compared the 10º with angles lower and higher. It is important to focus on the vorticity explained in chapter 1. There we can see the wake and the vortex on the trailing edge that generate this blue and yellow distortions.

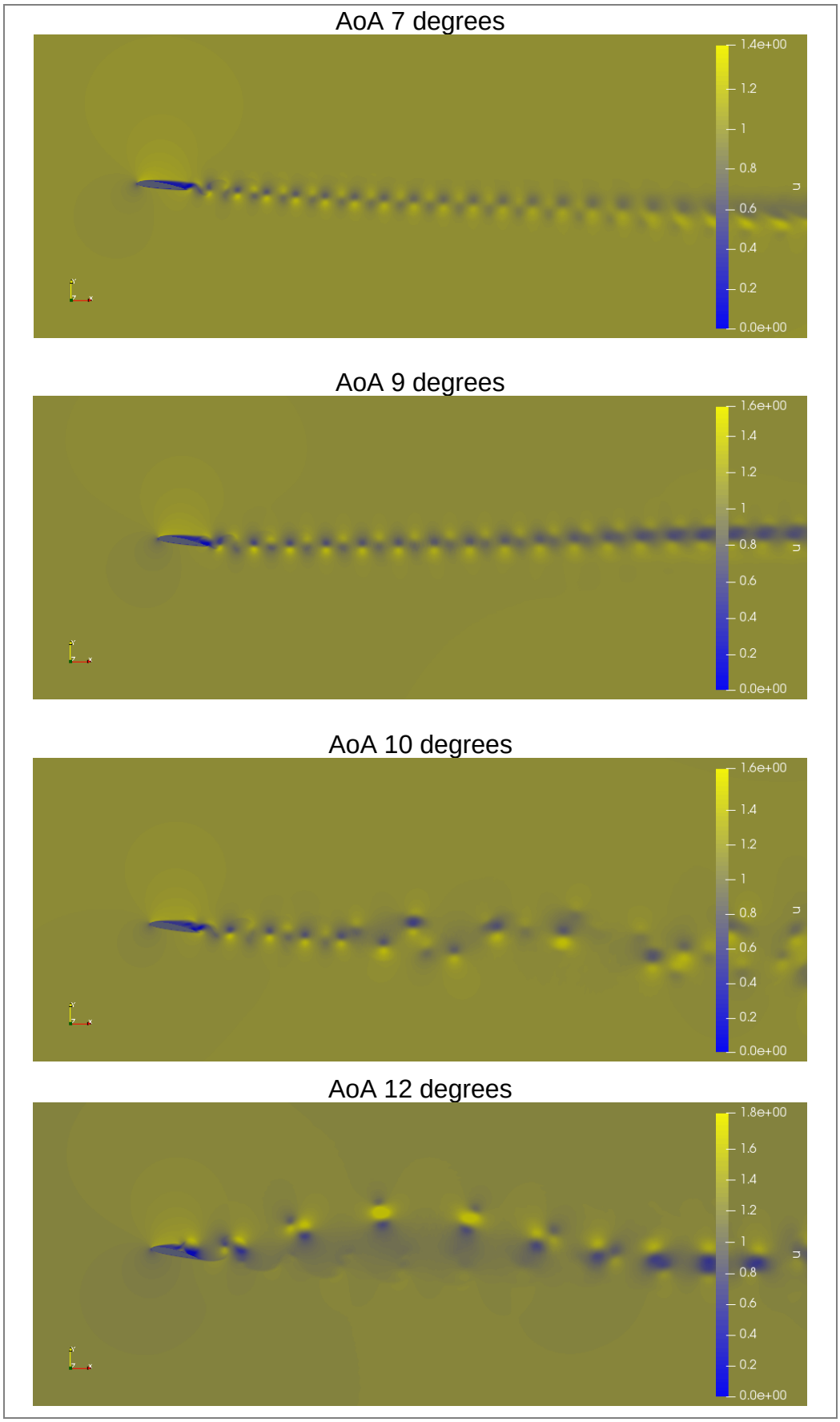

Figure 3.13: Vortex shedding comparation

From the simulations, we can observe clearly factors described and confirmed by the velocity and pressure field distribution.

On the first AoA, at 3 degrees, it is clearly observed how the boundary layer is attached to the airfoil and generates a wake that oscillates periodically. It is observed because the velocity field is constant and without perturbations from the leading to the trailing edge.

While the AoA is increasing, we arrive at 7º. Some detachment is detected since the 80% of the chord, but it is still a uniform wake and this is indicating us that the stall pint has not arrived yet.

Arriving at 9º, it is time to focus on the adverse pressure gradients generated around the 60% of the chord. Although it can recover and reattach the boundary layer with a minimum vortex. It is important to mention that it is not proportional the increasing of AoA with the appearing of vorticities.

In the next simulation we arrive at the critical range where the hysteresis has been detected. In figure 3.14, we can see those angles with a specific zoom on the airfoil in order to detect the point where the boundary layer is detached. About this, we can observe the detachment around the 50 and 60% of the chord. As well, how it is not enough strong to do the reattachment of the boundary layer, an unstable vortex shedding is generated.

This unstable vortex can be seen also in the same figure 3.14 where the flow is disturbed in the wake for 10º AoA and become quite stable but detached in 12º.

On the next simulations at 11 and 12 degrees we can see the airfoil starting with the boundary layer practically detached and the vortex shedding generated have to be recovered.

This is indicating us that at maximum 10 degrees of angle of attack the improvement lift systems have to be deployed. Systems like flaps, slats or activate the AFC in one of its multiple options.

AoA 7 degrees

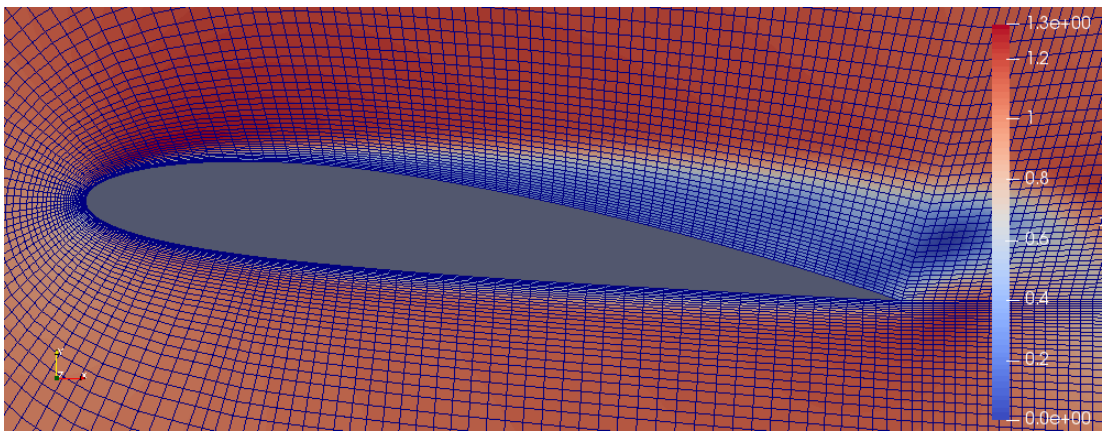

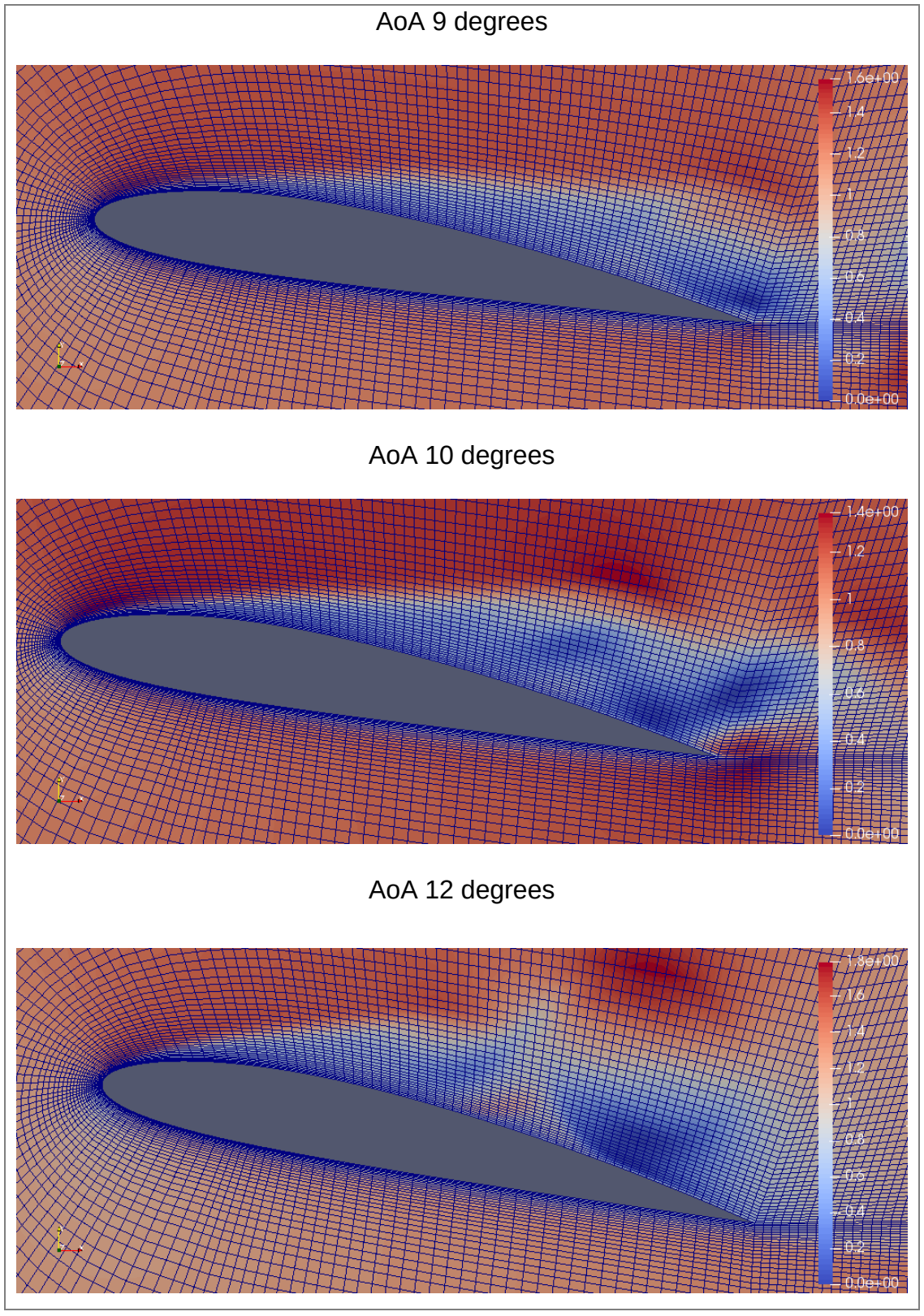

Figure 3.14: Specific velocity field around the airfoil

CHAPTER 4. ACTIVE FLOW CONTROL

4.1. AFC systems

As it has been told in the project, certain angle is necessary to implement some additional lift system in order to recover it at low speed. The purpose is to design a fluidic active flow control, avoiding conventional systems like flaps, slats, etc. These involve complex mechanical systems when they have to be deployed. Also, with new systems, weigh is reduced, an important factor in term of consumption and environmental saving. Firstly, we have to know what it is and how these kinds of systems work.

An active flow control allows us to handle the flow on a specific point. In this way we could redirect or modify it, obtaining a reattachment on the boundary layer and therefore, increase the lift at desired speed and angle. We can see a diagram in the figure 4.1 extracted from the study *"Active Flow Control: A Review"* of Mohsen Jahanmiri [12], where different phases of the process are interrelated until the necessity to implement some control elements. It shows how the boundary layer generates a drag force during the transition phase. Other part of the flow tries to reattach creating the bubbles on the wake, and other big part is separated and induces a very high lift reduction.

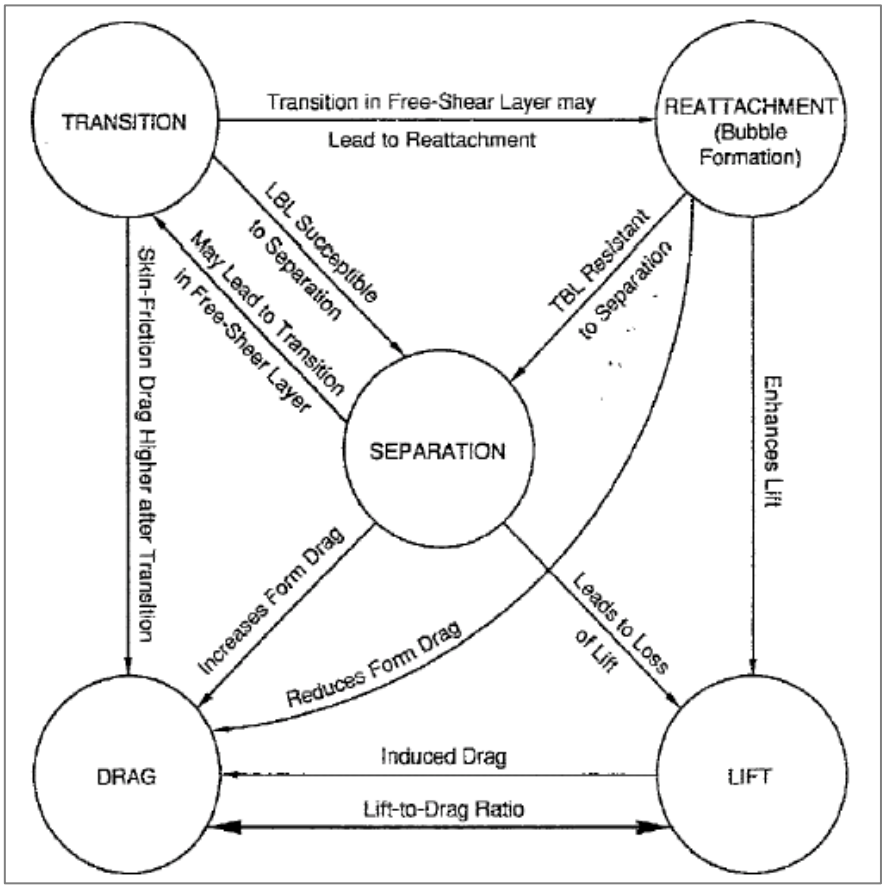

Figure 4.1: Flow control and lift loss interrelation

Once we need a flow control system, there are multiple solutions. First, as we see in the figure 4.2, we can have passive like conventional systems or active, our objective, that consist in actuate directly to the flow.

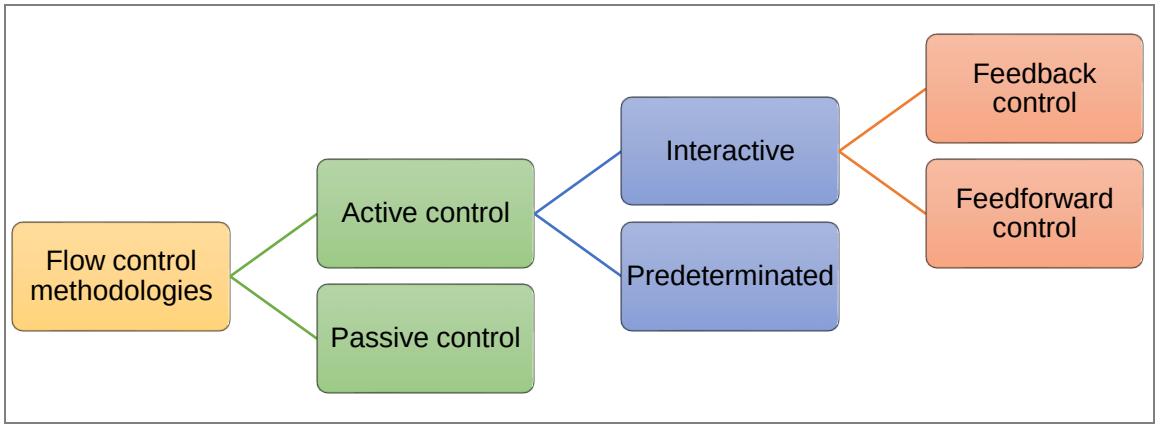

Figure 4.2: Flow control methods classification

Into the active flow we can find predeterminate that involves the introduction of steady or unsteady energy inputs without consideration for the state of the flow field. Otherwise, we can propose interactive methods of flow control where the power input to the actuator (controller) is continuously adjusted based on some form of measurement element (sensor). The control loop for interactive control can be either a feed forward (open) or feedback (closed) loop. In the feed forward control loop, the sensor is placed upstream of the actuator. In the last group we can find the control system proposed, a synthetic jet. This system was developed at Georgia Institute of Technology. This class of actuators uses an oscillatory surface within a cavity to generate a jet from the flow that is being controlled without the need for mass injection (Smith and Glezer, 1998). The jet was generated with a piezoelectric diaphragm in a periodic manner. Flow enters and exits the cavity through an orifice. We can see how it is in the figure 4.3.

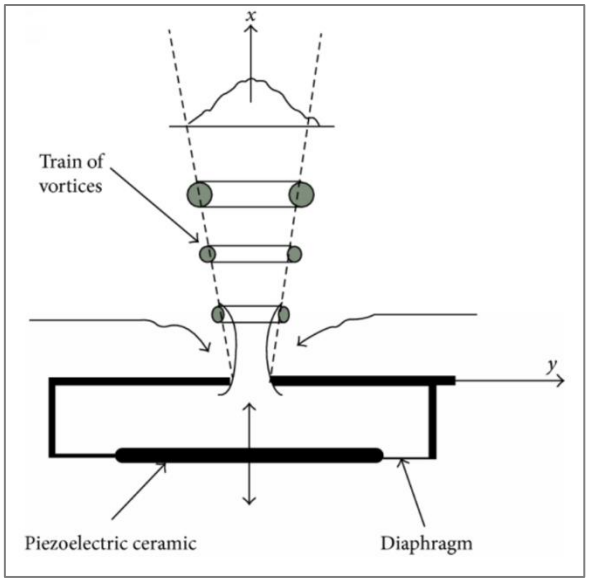

Figure 4.3: Synthetic jet actuator

4.2. AoA and jet location

As it was justified, the hysteresis problems are located around the 10º angle of attack. Therefore, the jet activation is produced when we arrive at this angle, achieving the objective of recover the angle and prevent the suddenly loss of lift.

The main idea is to recover the theorical lift coefficient diagram as we can see in figure 4.4 extracted from the study: “Experimental research on flow separation and control using synthetic jet actuators” wrote by E. Koopmans & H.W.M. Hoeijmakers [13]. In this one, there is an ideal representation, and in picture 4.5 we represent the desired diagram once the jet is activated for our particular case.

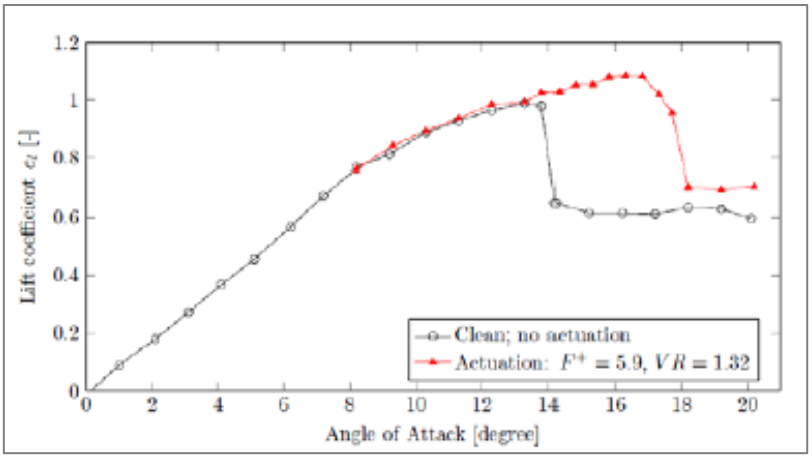

Figure 4.4: Jet actuator ideal graph

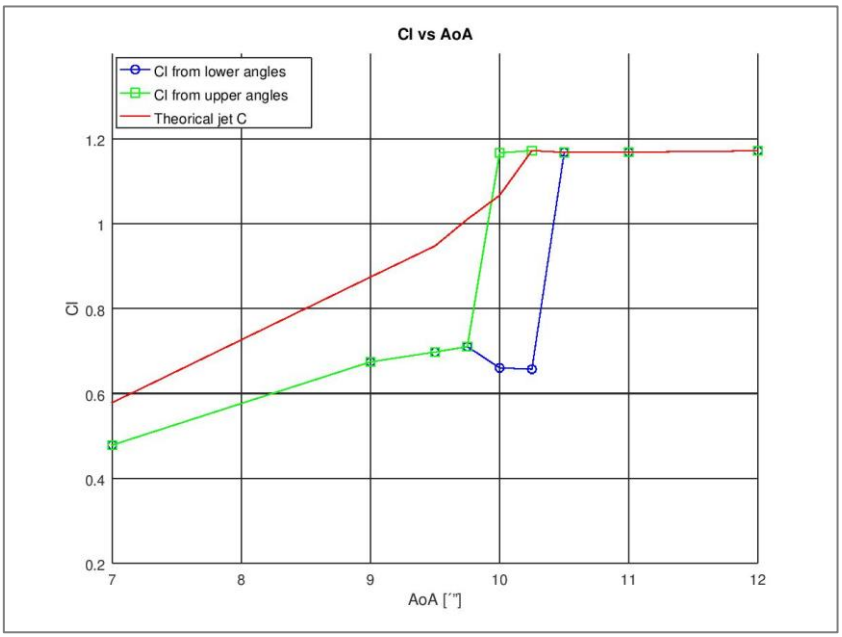

Figure 4.5: Theorical curve applied to NACA 2412 case with jet activated

With the jet activation we will get, in advance, a high recovery of lift that will make possible to avoid the leap and smooth the curve. Also, we could increase angle for maximum Cl with the consequent improvement in stall point.

Another improvement that we could find on CL vs AoA will be to reach the desired lift at lower AoA. In terms of graph, increasing slope.

In terms of location and design, as it has been explained, it should be installed around the 0.5 – 0.6c, at 0.55 c for the simulation. On the other hand, we have the jet thickness, in accordance with the selected system and the research about it, 0.03c is proposed for the mesh.

4.3. Mesh and conditions modifications

Once we have the AFC system that we want to implement and its parameters for location and width, the next step is to modify the mesh in gmsh in order to run the new simulations.

To do this, some variables has been introduced to take into account the jet. The idea was to make an intersection in two points on the airfoil upper wall. With this, we create another surface, thinner and more independent as we can see in the figure 4.6. This figure shows a zoom on the airfoil and the jet, later, a global view will be presented. A thinner mesh than the others is assigned to the jet surface in order to process the specific points. And, in conditions file, a velocity different of zero is established in “Y” axis, that is, perpendicular to the boundary layer.

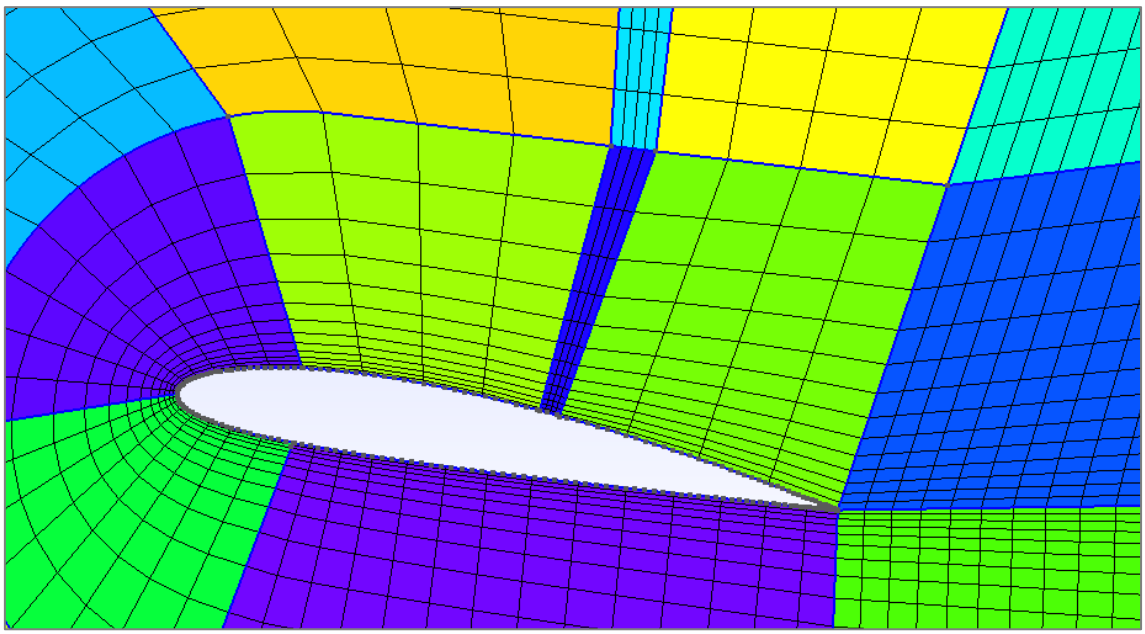

Figure 4.6: Jet result in gmsh

For obtaining this similarity to the jet, apart from adding it in the code, more modifications have been done, as it is seen in figure 4.7. After that, the opening angle of jet in the next surfaces was defined (figure 4.8) simulating how the jet is disturbed with the flow pass in “X” direction.

```
// JET
pj=.18; // jet location (in % of chord)
tj=.02; // jet thickness (in % of chord)

pjA=.55; // jet location (in % of chord)
tjA=.03; // jet thickness (in % of chord)
```

Figure 4.7: Jet implementation

```
ajf_n=75*Pi/180; // jet semi-opening angle forward nearfield (from airfoil)
ajb_n=70*Pi/180; // jet semi-opening angle backward nearfield (from airfoil)

ajf_m=(-2*Pi/180)+ajf_n+anf+daoau;
ajf_f=(-0*Pi/180)+ajf_m+amf+2*daoauu;
ajb_m=(-5*Pi/180)+ajf_n+anf+daoau;
ajb_f=(-8*Pi/180)+ajf_m+amf+2*daoauu;
```

Figure 4.8: Jet angle determination

Afterwards, we determinate the initial and final point for each part of the jet. Also, intersections and loops are added in order to generate new lines that will define the jet surfaces (figures 4.9 and 4.10). It is remarkable that it is only shown the loops that modify the final lines.

```
//LOOP OVER THE CHORD
//uasL = newl; Spline(uasL) = {teP,usP[{1:ij-1}],ujP}; CHANGED BY CENTRAL POINTS
ufsL = newl; Spline(ufsL) = {ujP,usP[{ij:#usP[]-1}],leP};
lasL = newl; Spline(lasL) = {teP,lsP[{1:ij-1}],ljP};
lfsL = newl; Spline(lfsL) = {ljP,lsP[{ij:#lsP[]-1}],leP};
ujfsL = newl; Spline(ujfsL) = {ujPf,usP[{ijfw:ij-1}],ujP};

//AFTER loop DEL TRAILING EDGE AL FINAL DEL JET

ujasL = newl; Spline(ujasL) = {teP,usP[{1:ijaf}],ujPa};

//ZONA CENTRAL ENTRE FW y AF JET

umasL = newl; Spline(umasL) = {ujPa,usP[{ijaf+1:ijfw-1}],ujPf};
```

Figure 4.9: Jet loops

```
//JET LOCATION CENTER, UPPER

xuj0 = -c+xj-ytj*Sin(thj); yuj0 = ycj+ytj*Cos(thj);
xuj = xte0+(xuj0-xte0)*Cos(aoa)+(yuj0-yte0)*Sin(aoa);
yuj = yte0-(xuj0-xte0)*Sin(aoa)+(yuj0-yte0)*Cos(aoa);
ujP=newp; Point(ujP)={xuj,yuj,0};
Printf("jet %g %g", xuj, yuj); //PRINT DEL JET

//FORWARD POINT

xuj0f = -c+xjf-ytjf*Sin(thjf); yuj0f = ycjf+ytjf*Cos(thjf);
xujf = xte0+(xuj0f-xte0)*Cos(aoa)+(yuj0f-yte0)*Sin(aoa);
yujf = yte0-(xuj0f-xte0)*Sin(aoa)+(yuj0f-yte0)*Cos(aoa);
ujPf=newp; Point(ujPf)={xujf,yujf,0};

//AFTER POINT

xuj0a = -c+xja-ytja*Sin(thja); yuj0a = ycja+ytja*Cos(thja);
xuja = xte0+(xuj0a-xte0)*Cos(aoa)+(yuj0a-yte0)*Sin(aoa);
yuja = yte0-(xuj0a-xte0)*Sin(aoa)+(yuj0a-yte0)*Cos(aoa);
ujPa=newp; Point(ujPa)={xuja,yuja,0};

//LOWER POINT
xlj0 = -c+xj+ytj*Sin(thj); ylj0 = ycj-ytj*Cos(thj);
xlj = xte0+(xlj0-xte0)*Cos(aoa)+(ylj0-yte0)*Sin(aoa);
ylj = yte0-(xlj0-xte0)*Sin(aoa)+(ylj0-yte0)*Cos(aoa);
ljP=newp; Point(ljP)={xlj,ylj,0};


dycdxte = 2*m/(p-1); dytdxte = 5*t*(a0/2+a1+2*a2+3*a3+4*a4);
dycdxle=2*m/p; thnfle=Atan(dycdxle)+Pi/2;
```

Figure 4.10: Jet points position implementation

Finally, the same as it was done with the original airfoil, lines are defined as transfinite and the mesh density as we can see in the figure 4.11. New control surfaces are generated and renamed.

```
//TRANSFINITE JET LINES TO SET NEW MESH CONDITIONS

jprognfld=Nnf;
jprogmfld=Nmf;
jprogffld=Nff;
jknfld=Kujnf;
jkmfld=Kujmf;
jkffld=Kujff;
nprog=5;
mprog=5;
fprog=5;
nldk=1.01;
mldk=1.01;
fldk=1.01;

//nearfield
Transfinite Line {ujfsL} = nprog Using Progression nldk;
Transfinite Line {ujasL} = nprog Using Progression nldk;
Transfinite Line {umasL} = nprog Using Progression nldk;
```

Figure 4.11: Mesh density

The final result of this process is a mesh as it is shown in the figure 4.12. This one is similar to the 4.6 but here, we can perfectly differentiate the nearfield, midfield and farfield regions. Also, the jet surface is clearly distinguished.

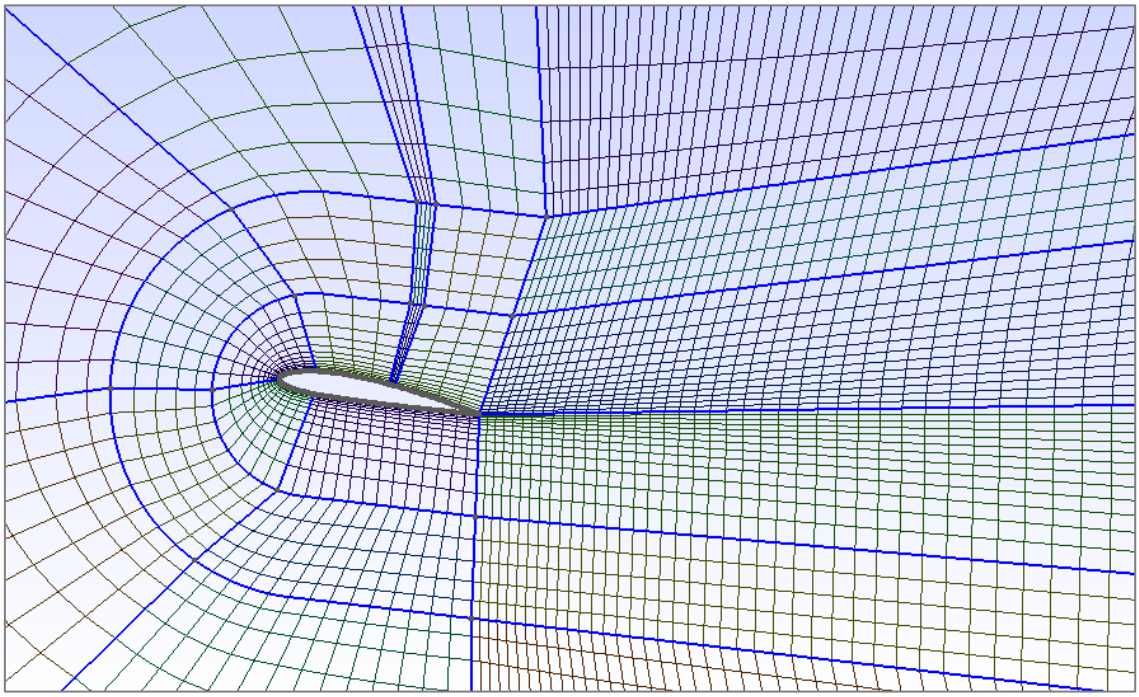

Figure 4.12: Jet Mesh

Once the .geo file is modified, it is time to realize the same with the conditions file. Principally, new surfaces are generated by the jet implementation and the initial conditions for them are modified as we can see on figures 4.13 and 4.14.

On boundary region, there are 3 new surfaces. These take into account the jet implementation and new boundary conditions for them have to be defined.

The boundary conditions, same as in chapter 2, but with the difference in the Jet region. This has been added to take into account a velocity different to 0 and with a direction perpendicular to the boundary layer.

```
<BOUNDARYREGIONS>
  <B ID="0"> C[1] </B> <!-- Inlet -->
  <B ID="1"> C[2] </B> <!-- Outlet -->
  <B ID="2"> C[3] </B> <!-- Upper Surface before jet -->
  <B ID="3"> C[4] </B> <!-- Jet -->
  <B ID="4"> C[5] </B> <!-- Upper Surface after jet -->
  <B ID="5"> C[6] </B> <!-- Lower Surface -->
  <B ID="6"> C[7] </B> <!-- Upper Boundary -->
  <B ID="7"> C[8] </B> <!-- Lower Boundary -->
</BOUNDARYREGIONS>
```

Figure 4.13: Boundary regions definition

```
<REGION REF="2">
  <D VAR="u" VALUE="0" />
  <D VAR="v" VALUE="0" />
  <N VAR="p" USERDEFINEDTYPE="H" VALUE="0" />
</REGION>
<REGION REF="3"> <!--JET REGION -->
  <D VAR="u" VALUE="0" />
  <D VAR="v" VALUE="1" />
  <N VAR="p" USERDEFINEDTYPE="H" VALUE="0" />
</REGION>
<REGION REF="4">
  <N VAR="u" VALUE="0" />
  <D VAR="v" VALUE="0" />
  <N VAR="p" USERDEFINEDTYPE="H" VALUE="0" />
</REGION>
```

Figure 4.14: Jet boundary initial conditions

For closing this section, it is important to say that the processing time and steps as been reduced in order to run the jet mesh density.

4.4. AFC simulation results

This section should be to show the jet results similar as the original related with hysteresis point. Due to the time waste proving the hysteresis existence, that finally was the main aim for the project. Adding the inconvenience of defining and running the simulation for a cambered airfoil, the simulation results cannot be possible to process. An extract of the main problem related to the file running is shown in the figure 4.15. Also, we can observe how the steps has been reduced and the initial conditions done with an existing field in order to simplify and be able to simulate but it has not been possible.

```
================================================================================
Initial Conditions:
  - Field u: from file NACA9AoA_40.chk
  - Field v: from file NACA9AoA_40.chk
  - Field p: from file NACA9AoA_40.chk
Writing: "NACA10AoA_JET_40.chk" (0s, XML)
Steps: 5        Time: 50.0005      CPU Time: 293.979s
Steps: 10       Time: 50.001       CPU Time: 1.36163s
Writing: "NACA10AoA_JET_41.chk" (0s, XML)
Steps: 15       Time: 50.0015      CPU Time: 1.59438s
Steps: 20       Time: 50.002       CPU Time: 1.67202s
Writing: "NACA10AoA_JET_42.chk" (0s, XML)
Steps: 25       Time: 50.0025      CPU Time: 1.48107s
Steps: 30       Time: 50.003       CPU Time: 1.35101s
Writing: "NACA10AoA_JET_43.chk" (0s, XML)
Steps: 35       Time: 50.0035      CPU Time: 1.42311s
Steps: 40       Time: 50.004       CPU Time: 1.37592s
Writing: "NACA10AoA_JET_44.chk" (0s, XML)
Steps: 45       Time: 50.0045      CPU Time: 1.42597s
Steps: 50       Time: 50.005       CPU Time: 1.49341s
Writing: "NACA10AoA_JET_45.chk" (0s, XML)

Fatal   : Level 0 assertion violation
NaN found during time integration.
```

Figure 4.15: Jet simulation summary

CONCLUSIONS

The main conclusion is the necessity of a flow control system when we reach angles of attack that generates detachment on the boundary layer and vortex shedding. In addition, with the hysteresis detection and analysis, the project has been reconducted and a specific angle and location have been determinate to design the fluidic active flow control.

Continuing the last paragraph, I refer to the conclusion about hysteresis where we probed that in a NACA2412 airfoil, approximated from a supercritical and with approach speed, exist hysteresis around the 10 degrees Angle of Attack.

Other important conclusion is how the hysteresis can affect to the airfoil. The suddenly increasing or decreasing of lift is a big problem in order to stabilize the airfoil. Nowadays, you can trim or fix a specific angle, so you can be able to fix an angle that is common in critical phases of flight, avoiding problems related with the hysteresis.

About the active flow control, it is a method that can reduce weight and maintenance tasks. But the main problem is to certificate the system for accomplish airworthiness required for the aviation organizations.

Talking about the final chapter, it is interesting for next projects to continue developing the active flow control for cambered airfoils and extend it to more complex airfoils or with data point of SC airfoils.

As a personal growth, this study has given me the opportunity to improve my knowledge in computational software and study this kind of systems. Those were unknown for my when I started to research. In this way, it is important to continue developing systems that improve the efficiency of the aircraft because consequently we are saving economic and environmental costs.

BIBLIOGRAPHY

[1] Basharat Ali Haider, Naveed Durrani, Nadeem Aizud and Salimuddin Zahir. “Aerodynamic Stall Control of a Generic Airfoil using Synthetic Jet Actuator”. World Academy of Science, Engineering and Technology International Journal of Aerospace and Mechanical Engineering Vol:4, No:9, 2010

[2] NASA Dryden Technology Facts – “The Supercritical Airfoil”. TF-2004-13-DFRC

[3] Ahmad Batikh, Lucien Baldas, Stéphane Colin. “APPLICATION OF ACTIVE FLOW CONTROL ON AIRCRAFTS - STATE OF THE ART”. Institut Clément Ader (ICA), Université de Toulouse, CNRS-INSA-ISAE-Mines Albi-UPS, Toulouse, France

[4] United States Air Force. US Air Force Fact Sheet: C-17 Globemaster III. https://www.af.mil/About-Us/Fact-Sheets/Display/Article/1529726/c-17-globemaster-iii/

[5] ENAIRE. Annex IV - AIP Barcelona Airport (2007)

[6] Mueller, T. J., “The influence of laminar separation and transition on low Reynolds number airfoil hysteresis”. Journal of Aircraft, Vol. 22, No. 9, 1985, pp763-770.

[7] Xiong, Zhixun, Zhenbing, Lin. “A novel optimal design for an application-oriented synthetic jet actuator” National Natural Science Foundation of China. https://www.sciencedirect.com/science/article/pii/S1000936114000727

[8] Nektar++ tutorials, Chapter 8, Incompressible Navier-Stokes http://doc.nektar.info/userguide/4.2.0/user-guidech9.html#x39-1450008

[9] Universidad del Pais vasco. Analisis y modelado en CFD. https://www.ehu.eus/es/web/get/eskainitako-zerbitzuak

[10] https://fyfluiddynamics.com/post/55175429601/flow-around-an-airfoil-with-a-leading-edge-slat-is

[11] www.airfoiltools.com

[12] Jahanmiri, Mohsen, “Active Flow Control: A review”. Chalmers university of technology. Göteborg, Sweden, 2010.

[13] E. Koopmans*& H.W.M. Hoeijmakers, “Experimental research on flow separation ncontrol using synthetic jet actuators”. University of Twente, Enschede, Netherlands.

[14] Zifeng Yang; Hirofumi Igarashi; Mathew Martin; Hui Hu (Jan 7–10, 2008). “*An Experimental Investigation on Aerodynamic Hysteresis of a Low-Reynolds Number Airfoil*”. 46th AIAA Aerospace Sciences Meeting and Exhibit. Reno, Nevada: American Institute of Aeronautics and Astronautics. AIAA-2008-0315.